

Anion Capture and Exchange by Functional Coatings: New Routes to Mitigate Steel Corrosion in Concrete Infrastructure

Gabriel Falzone (*, †), Magdalena Balonis (†, ‡, ††), Dale Bentz (‡), Scott Jones (‡), Gaurav Sant (*, **, ††)

Abstract

Chloride-induced corrosion is a major cause of degradation of reinforced concrete infrastructure. While the binding of chloride ions (Cl^-) by cementitious phases is known to delay corrosion, this approach has not been systematically exploited as a mechanism to increase structural service life. Recently, Falzone et al. [*Cement and Concrete Research* **72**, 54-68 (2015)] proposed calcium aluminate cement (CAC) formulations containing NO_3^- -AFm to serve as *anion exchange coatings* that are capable of binding large quantities of Cl^- ions, while simultaneously releasing corrosion-inhibiting NO_3^- species. To examine the viability of this concept, Cl^- binding isotherms and ion-diffusion coefficients of a series of hydrated CAC formulations containing admixed $\text{Ca}(\text{NO}_3)_2$ (CN) are quantified. This data is input into a multi-species Nernst-Planck (NP) formulation, which is solved for a typical bridge-deck geometry using the finite element method (FEM). For exposure conditions corresponding to seawater, the results indicate that Cl^- scavenging CAC coatings (i.e., top-layers) can significantly delay the time to corrosion (e.g., $5 \leq d_f \leq 10$, where d_f is the steel corrosion initiation delay factor [unitless]) as compared to traditional OPC-based systems for the same cover thickness; as identified by thresholds of Cl^-/OH^- or $\text{Cl}^-/\text{NO}_3^-$ (molar) ratios in solution. The roles of hindered ionic diffusion, and the passivation of the reinforcing steel rendered by NO_3^- are also discussed.

Keywords: (C) corrosion; (C) finite element analysis; (D) calcium aluminate cement; (D) chloride; (-) calcium nitrate

* Laboratory for the Chemistry of Construction Materials (LC²), Department of Civil and Environmental Engineering, University of California, Los Angeles, CA, USA

† Department of Materials Science and Engineering, University of California, Los Angeles, CA, USA

‡ Technology Strategist, Institute for Technology Advancement, University of California, Los Angeles, CA, USA

§ Engineering Laboratory, National Institute of Standards and Technology, Gaithersburg, MD, USA

** California Nanosystems Institute (CNSI), University of California, Los Angeles, CA, USA

†† Corresponding authors: M. Balonis (mbalonis@ucla.edu) and G. Sant (Email: gsant@ucla.edu)

36 **1. Introduction and background**

37 Chloride (Cl^-) induced corrosion of reinforcing steel is a significant cause of premature damage
38 and degradation of concrete infrastructure [1–3]. Concrete may be subject to chloride ingress as
39 a result of contact with de-icing salts, seawater exposure, etc. [4]. In the U.S. alone, over \$8 billion
40 is spent annually on corrosion-related repair, maintenance, and rehabilitation of bridges [5]. In
41 addition, 11 % of the 600,000 highway bridges in the U.S. are deemed to be structurally deficient
42 [5,6]; the majority due to corrosion-related degradation.

43
44 Due to the alkalinity of cementitious pore solutions, steel embedded in concrete is generally
45 covered with a passivating oxide layer ($\gamma\text{-Fe}_2\text{O}_3$ [7,8]). The ingress of Cl^- ions into the concrete is
46 thought to initiate steel corrosion by displacing OH^- from this passivating layer [2,9]. Cl^- -induced
47 depassivation results in localized pitting and corrosion product formation, which reduces the
48 cross-sectional area of the reinforcing steel, and, therefore, its load-bearing capacity [3,7,9]. The
49 Cl^-/OH^- ratio (in molar units), which accounts for the passivating effects of OH^- ions, is often used
50 to describe the risk of steel corrosion [9,10]. Although the precise value of Cl^-/OH^- required to
51 initiate corrosion is a subject of debate [9,10], a survey of the literature suggests that corrosion
52 initiates when $\text{Cl}^-/\text{OH}^- \geq 0.6$ [9–11].

53
54 The presence of NO_3^- and NO_2^- anions in the pore solution can counteract the corrosive actions
55 of Cl^- ions [12–17]. These species mitigate corrosion processes by oxidizing Fe^{2+} species to Fe^{3+}
56 ions, which precipitate and re-form passivating films [7,18]. A critical $\text{Cl}^-/\text{NO}_2^-$ ratio for corrosion
57 initiation has been suggested to range from 0.25-to-2.0 (unitless, molar ratio) [19,20]. While data
58 regarding NO_3^- is lacking, indirect evidence suggests that NO_3^- provides similar corrosion
59 inhibition as NO_2^- (i.e., for $\text{Cl}^-/\text{NO}_3^- \leq 0.25$) [21]. While the use of NO_2^- or NO_3^- is valuable, the
60 corrosion inhibition offered by these species offer is often limited by their initial dosage into the
61 concrete [22]. Moreover, both $\text{Ca}(\text{NO}_3)_2$ and $\text{Ca}(\text{NO}_2)_2$ are highly soluble and, therefore, are
62 subject to leaching, which may reduce their potential for corrosion mitigation.

63
64 The binding of Cl^- by cementitious phases can significantly suppress Cl^-/OH^- in the pore solution
65 and thereby increase the service life of infrastructure [23–25]. For example, Cl^- binding can occur
66 by ion exchange into alumino-ferrite monosubstituent (AFm) compounds, or by sorption onto C-
67 S-H or other compounds [26]. AFm's are represented by $[\text{Ca}_2(\text{Al,Fe})(\text{OH})_6] \cdot \text{X} \cdot n\text{H}_2\text{O}$, where X is the
68 exchangeable interlayer anion, and n is the number of water molecules. The site (i.e., anion)
69 occupation preference within the AFm-interlayer has the ranking $\text{Cl}^- > \text{NO}_3^- > \text{NO}_2^- > \text{CO}_3^{2-} > \text{SO}_4^{2-}$
70 $> \text{OH}^-$ [27], assuring that AFm's present in cementitious formulations (i.e., those containing CO_3^{2-}
71 , SO_4^{2-} , or OH^- in their interlayers) will capture Cl^- ions from solution to form Cl-AFm (i.e., Friedel's
72 salt) or Kuzel's salt [27,28]. Ion exchange results in the release of the anion initially present in the
73 AFm interlayer by a process of anion capture and exchange (ACE); a process that is guided by
74 thermodynamic selectivity [27,28].

75
76 ACE by AFm's is significant as (i) it operates in a Cl^- concentration range relevant to typical ingress
77 conditions (≈ 14 mmol/L [29]), (ii) it has a much larger binding capacity per unit mass than Cl^-
78 sorption by C-S-H [25], and (iii) Cl^- species taken up by AFm's are more strongly bound into their
79 structure (i.e., reflecting structural incorporation), than binding by the C-S-H which represents

80 weaker physisorption. Therefore, the Cl^- binding capacity of cementitious formulations is linked
81 to the mass fraction of AFm phases present [30]. Even though the specific binding capacity of
82 AFm phases is high, the total binding capacity of OPC-based formulations is limited, since AFm's
83 comprise only 5 % to 15 % by mass of the solids in a hydrated OPC binder, offering only limited
84 retardation of steel corrosion [19,23–25]. The Cl^- binding capacity of OPC-based binders can be
85 increased by the addition of supplementary cementing materials (SCMs: e.g., ground-granulated
86 blast-furnace slag [31,32], fly ash [33]) which increases the $\text{Al}_2\text{O}_3/\text{SO}_3$ ratio of the mixture, leading
87 to the enhanced formation of AFm's at the expense of AFt [19,34,35]. However, these effects are
88 confounded with changes in the transport properties (e.g., permeability, and diffusivity) and the
89 limited reaction of the SCMs that become relevant when OPC is replaced by SCMs at high levels
90 [25,34,36]. As a result, while SCMs do indeed contribute reactive alumina that is required for
91 AFm formation, they do so at a level that only slightly increases the mass of AFm's formed.

92
93 Several numerical models have been developed to describe mass transport of ions that influence
94 the service life of reinforced concrete infrastructure [23,24,37–42]. These transport models vary
95 in complexity from single-species models governed by Fick's laws of diffusion [23,37], to multi-
96 species Poisson-Nernst-Planck (PNP) models which account for electric coupling between ions
97 due to their differing mobilities [40,41]. Other models may also consider the effect of advective
98 transport due to moisture gradients (e.g., replicating the effects of wet-dry cycles) [43,44] and/or
99 reactions between ions and cementitious solids, which may be accounted for by mass-transport
100 and chemical equilibrium calculations [40,41,45], or by considering sorption isotherms
101 [23,24,37,46]. A wide-range of models especially describe the role of Cl^- binding by cementitious
102 phases on service life predictions [23,24]. Although quantitative prediction of the service lifetime
103 of real structures is notoriously difficult, carefully formulated transport models can illustrate the
104 role of enhanced Cl^- binding by cementitious compounds on delaying the onset of corrosion.

105
106 Calcium aluminate cement (CAC) mixtures, when suitably formulated, can exhibit a significantly
107 higher Cl^- binding capacity as compared to those of OPC systems [47]. However, this approach
108 has not been studied as a pathway to mitigate corrosion due to a lack of clarity as to how AFm
109 formation can be increased in a controlled manner to scavenge/sequester Cl^- species. Recently,
110 Falzone et al. suggested that NO_3^- -AFm dominant hydrated CAC mixtures (e.g., those containing
111 up to 60 mass % AFm) could produce ACE benefits, by sequestering Cl^- ions while simultaneously
112 releasing NO_3^- (or NO_2^-) species, i.e., an anodic corrosion inhibitor [28]. This *smart release* of NO_3^-
113 and NO_2^- ions was first described by Balonis and Glasser [19]. Significantly, since volume changes
114 accompanying NO_3^- to Cl^- exchange in the AFm's are minimal, no internal damage develops, e.g.,
115 due to deleterious shrinkage or expansion [48]. With this concept in mind, this study investigates
116 the efficacy of CAC + $\text{Ca}(\text{NO}_3)_2$ based *top-layers* (i.e., formed by replacing a fractional thickness
117 of the OPC concrete cover) that engender ACE as a means to delay corrosion. CAC-based binders
118 are restricted to a top-layer due to their high cost ($\approx 5x$ that of OPC). The beneficial effects of Cl^-
119 binding (i.e., reduced Cl^- abundance around the steel reinforcement) and NO_3^- ion release are
120 explained by considering thermodynamic and transport properties that are influential in the
121 initiation and progression of corrosion. As such, this study explains how ACE is an impactful
122 pathway to delay corrosion degradation of infrastructure and thereby prolong service life.

123

124 **2. Materials and methods**

125 **2.1 Materials**

126 A commercially available calcium aluminate cement (Secar[®]51 produced by Kerneos Aluminate
127 Technologies)¹ was used. The oxide composition of the CAC as determined by X-ray fluorescence
128 (XRF) was (51.05 ± 0.20) % Al₂O₃, (38.94 ± 0.40) % CaO, (4.77 ± 0.40) % SiO₂, (2.23 ± 0.10) % Fe₂O₃,
129 (2.02 ± 0.01) % TiO₂, (0.59 ± 0.10) % MgO, (0.11 ± 0.01) % P₂O₅, (0.31 ± 0.04) % K₂O and (0.07 ±
130 0.03) % Na₂O by mass [49]. Unless otherwise noted, the uncertainty represents one standard
131 deviation. The mineralogy of the CAC as determined by X-ray diffraction and Rietveld refinement,
132 was 73.3 ± 3.3 % CA, 18.1 ± 3.3 % C₂AS, 4.9 ± 2.0 % CT with minor phases in the form of 0.8 %
133 CaO, 0.6 % C₂F, 1.5 % C₃FT and 0.8 % Fe₃O₄ by mass [50].

134
135 CAC pastes were prepared at a fixed water-to-cement ratio ($w/c = 0.45$, mass basis) using de-
136 ionized (DI) water, as described in ASTM C305 [51]. Calcium nitrate (Ca(NO₃)₂, CN) was added to
137 the CAC mixtures in dosages of 0 %, 10 %, and 30 % by mass of anhydrous CAC. The CN admixture
138 was provided in the form of an aqueous solution (52 mass % CN in water). This admixture was
139 first combined with additional water prior to mixing with the anhydrous CAC. CAC mortars were
140 also prepared at the same CN dosages using ASTM C778 [52] compliant graded quartz sand at
141 volume fractions $\phi_q = 0.00, 0.25, \text{ and } 0.50$. To suppress the formation of metastable hydrates
142 [53,54], the mixtures were cured under sealed conditions at 45 °C ± 0.2 °C for a period of 28 d.
143 Reagent grade calcium chloride dihydrate (CaCl₂·2H₂O, > 99 % purity) was added to Milli-Q water
144 (i.e., 18 MΩ·cm deionized water) to prepare solutions at Cl⁻ concentrations of: 0.01, 0.05, 0.1,
145 0.3, 1, and 3 mol/L.

146
147 **2.2 Methods**

148 **2.2.1 Thermodynamic calculations**

149 To ascertain the phase assemblages of the CAC mixtures prepared in Section 2.1, thermodynamic
150 calculations were carried out using the Gibbs Energy Minimization Software⁷ (GEMS-PSI), version
151 2.1 [55–58]. Thermodynamic modeling was performed for systems containing CAC (Secar[®]51) for
152 $w/c = 0.45$, and for the three CN dosages listed above [28]. The calculations were carried out at
153 $p = 101 \text{ kPa}$ and $T = 45 \text{ °C}$, with the solid and liquid phases being set to equilibrium with CO₂-free
154 air. The predicted CAC phase assemblages represent mature CAC pastes in which the formation
155 of metastable hydrates CAH₁₀ and C₂AH₈ is suppressed [54]. The calculations account for the
156 partial reaction of the anhydrous CAC, to obtain phase assemblages as a function of degree of
157 CAC hydration. The thermodynamic properties of solid and aqueous species were sourced from
158 the GEMS-PSI database, and amended with additional information sourced from the literature
159 for CACs [26,27,48,59–63]. Falzone et al. [28] contains further details and a compilation of the
160 thermodynamic properties of compounds relevant to the simulations. Qualitative agreement
161 between GEMS-predicted and experimental phase assemblages for both plain and CN-dosed CAC

¹ Certain commercial products are identified in this report to specify the materials used and procedures employed. In no case does such identification imply endorsement or recommendation by the University of California, Los Angeles or the National Institute of Standards and Technology, nor does it indicate that the products are necessarily the best available for the purpose.

162 mixtures has already been established (via X-ray diffraction and thermogravimetric analysis)
163 elsewhere [28].

164 2.2.2 *Cl⁻ binding isotherms*

166 After 28 d of curing, to minimize transport hindrances on chloride binding, the hydrated CAC
167 pastes were crushed to a fine powder, sieved ($d \leq 63 \mu\text{m}$, d is the particle diameter) and used in
168 Cl^- binding experiments at $25 \text{ }^\circ\text{C} \pm 3 \text{ }^\circ\text{C}$. Cl^- binding isotherms of CAC pastes dosed with CN
169 admixture (0 %, 10 %, and 30 % by mass) were quantified using the equilibrium method [46].
170 Triplicate powdered CAC pastes ($m_{\text{paste}} = 30 \text{ g}$) were immersed in CaCl_2 solutions ($V_{\text{sol}} = 0.1 \text{ L}$)
171 prepared across a range of concentrations [25]. CaCl_2 was selected to minimize the potential for
172 cation-dependent alterations to the hydrated phase assemblages, and to provide sufficient Ca^{2+}
173 ions required for the formation of Friedel's salt from hydrogarnet (C_3AH_6) [29,64]. Following
174 immersion of CAC pastes in CaCl_2 solutions, the free Cl^- concentration ($C_{\text{Cl},f}$) in solution was
175 measured at 7 d time-intervals over a 21 d period. A multi-parameter benchtop meter (Orion
176 VersaStar, ThermoScientific¹) that was provided with a Cl^- selective electrode (ISE; 9617BNWP,
177 ThermoScientific¹) was used to measure $C_{\text{Cl},f}$.

178
179 The ISE was calibrated using calibration solutions prepared using Milli-Q water + $\text{CaCl}_2 \cdot 2\text{H}_2\text{O}$ over
180 the concentration range $0.001 \text{ mol/L} \leq C_{\text{Cl},f}^0 \leq 3 \text{ mol/L}$, at $25 \text{ }^\circ\text{C} \pm 3 \text{ }^\circ\text{C}$. To perform the binding
181 measurements, $\approx 5 \text{ mL}$ of solution was extracted, and filtered using a syringe fitted with a $0.2 \mu\text{m}$
182 filter to remove solids. The extracted solution was diluted in 100 mL Milli-Q water, and acidified
183 using 0.3 mol/L HNO_3 to adjust the pH to a range of $3 \leq \text{pH} \leq 4$, as required to meet operational
184 specifications of the ISE. The pH was measured using a ThermoScientific Ross Ultra electrode¹
185 calibrated using buffer solutions over the range $3 \leq \text{pH} \leq 13$ at $25 \text{ }^\circ\text{C} \pm 3 \text{ }^\circ\text{C}$. To minimize any ionic
186 interferences on the concentration measurement, the solution was then dosed with a suitable
187 amount of ionic strength adjuster (ISA; 2 mL ISA per 100 mL solution), following which $C_{\text{Cl},f}$ was
188 measured using a Cl^- specific ISE.

189 2.2.3 *Static light scattering*

191 Since solid surface area influences binding isotherms, the particle size distributions (PSDs) of the
192 crushed CAC pastes were determined by static light scattering (SLS). An SLS particle analyzer
193 (LS13-320, Beckman Coulter¹) was used to assess the surface area, using isopropyl alcohol (IPA)
194 as the carrier fluid. Prior to their characterization, each powder was added to IPA and
195 ultrasonicated to ensure its dispersion to primary particles. The complex refractive indices of the
196 IPA and hydrated CAC pastes were taken as $n_{\text{IPA}} = 1.37 + 0.00i$ [65] and $n_{\text{CAC}} = 1.70 + 0.10i$ [66],
197 respectively. The maximum uncertainty in the median diameter (d_{50}) was around 6 % based on 6
198 replicate measurements. The d_{50} of the powdered CAC pastes were nominally similar and on the
199 order of $1.3 \mu\text{m}$, $1.1 \mu\text{m}$, and $2.5 \mu\text{m}$ for the 0 % CN, 10 % CN, and 30 % CN mixtures, respectively.
200 The densities of these mixtures were estimated as 1700 kg/m^3 , 1900 kg/m^3 , and 2000 kg/m^3 ,
201 respectively, based on the thermodynamic calculations. The specific surface areas of the powders
202 were estimated as $150 \text{ m}^2/\text{kg}$, $250 \text{ m}^2/\text{kg}$, and $50 \text{ m}^2/\text{kg}$, respectively, assuming spherical
203 particles.

204

205 **2.2.4 Electrical impedance spectroscopy**

206 Electrical impedance spectroscopy was used to assess ion-diffusion in hydrated CAC pastes and
 207 mortars based on measurements of their bulk resistance (R_b , ohms) [67]. Custom conductivity
 208 cells were fabricated by modifying cylindrical polystyrene containers (diameter = 53.9 mm, height
 209 = 47.6 mm). Precision-ground 316 stainless steel rods (diameter = 3.18 mm \pm 0.01 mm) served as
 210 parallel electrodes spanning the entire height of the container, at a center-to-center separation
 211 of 25.4 mm \pm 0.5 mm. The geometry factor (k , m⁻¹) of each cell was determined by calibrating the
 212 measured conductivity to reference NaOH solutions in DI-water (0.1 % and 5 % by mass).

213
 214 Hydrated CAC compositions dosed with 0 %, 10 %, 30 % by mass CN and containing different
 215 volume fractions of graded quartz sand (ϕ_q = 0.00, 0.25, 0.50) were cast into these cells, sealed,
 216 and cured for 28 d at 45 °C \pm 0.2 °C; and their bulk electrical conductivity measured in duplicate.
 217 EIS spectra were obtained using a Solartron Analytical 1287 Electrochemical Interface¹ with a
 218 1252A Frequency Response Analyzer using an AC input signal of 100 mV. A frequency range of
 219 10⁻¹-to-10⁵ Hz was sampled with 10 points recorded per decade.

220
 221 The effective diffusion coefficient of an ionic species in a cementitious microstructure is related
 222 to its bulk conductivity (σ_{eff} , i.e., equivalent to inverse resistivity), and to the conductivity of the
 223 solution saturating its pores (σ_0) as described by the Nernst-Einstein relation [68]:

$$D_i = D_i^{inf} \frac{\sigma_{eff}}{\sigma_0} \quad (1)$$

224 where, D_i^{inf} is the diffusion coefficient of the i^{th} species at infinite dilution in water. This approach
 225 was used to account for transport hindrances on chloride (and on nitrate transport), as would be
 226 applicable to real concrete systems. As a significant quantity of pore solution from the hydrated
 227 CAC pastes [69] could not be obtained, the pore solution conductivity (σ_0) of CAC mixtures
 228 (without CN) was calculated based on the initial pore solution concentrations ($I_M \leq 30$ mmol/kg,
 229 see Table 1) obtained from GEMS using the Kohlrausch limiting law, with electrochemical activity
 230 corrections carried out using the extended Debye-Hückel relation [70]. The conductivity of the
 231 pore solutions of the 10 mass % CN and 30 mass % CN mixtures was estimated by performing EIS
 232 on solutions with CN dosage equivalent to their mixing water, as the conductivity is expected to
 233 be dominated by the abundant CN species.

234
 235
 236 **3. Results**

237 **3.1 Thermodynamic calculations**

238 Following on from Falzone et al. [28], Figure 1 shows calculated phase assemblages for CAC
 239 pastes ($w/c = 0.45$) containing different dosages of CN admixture (0-to-30 mass % CN). In the
 240 plain CAC paste (0 % CN, Figure 1a) C_3AH_6 , C_2ASH_8 , and $Al(OH)_3$ are noted as the predominant
 241 hydrated phases. These calculations consider a “mature” CAC paste, meaning that metastable
 242 hydrates that could be present at early ages (e.g., CAH_{10} , C_2AH_8) are not expected to exist as they
 243 convert, in time (i.e., at equilibrium), to C_3AH_6 and $Al(OH)_3$. When CAC is admixed with a sufficient
 244 dosage (30 mass % of CN), C_3AH_6 and C_2ASH_8 formation is entirely suppressed in favor of NO_3 -
 245 AFm (see Figure 1c). At intermediate CN dosages (e.g., 10 % CN; Figure 1b), the phase assemblage
 246 demonstrates an intermediate composition, containing a mixture of NO_3 -AFm, C_2ASH_8 , and

247 C_3AH_6 . These systems are all expected to demonstrate substantial capacity for Cl^- binding, in
 248 proportion to their CN dosage. It should be noted that the systems evaluated are water-deficient,
 249 meaning that reaction would cease before all the anhydrous CAC is consumed. This is significant
 250 as any unhydrated CAC present, in relation to its content, during binding studies (see Section 3.2)
 251 will sequester Cl^- by the formation of Friedel's salt. Furthermore, the porosity of the CAC pastes
 252 is expected to decrease as the CN dosage increases, due to the larger molar volume of the AFm
 253 compounds in comparison to that of C_3AH_6 [28].
 254

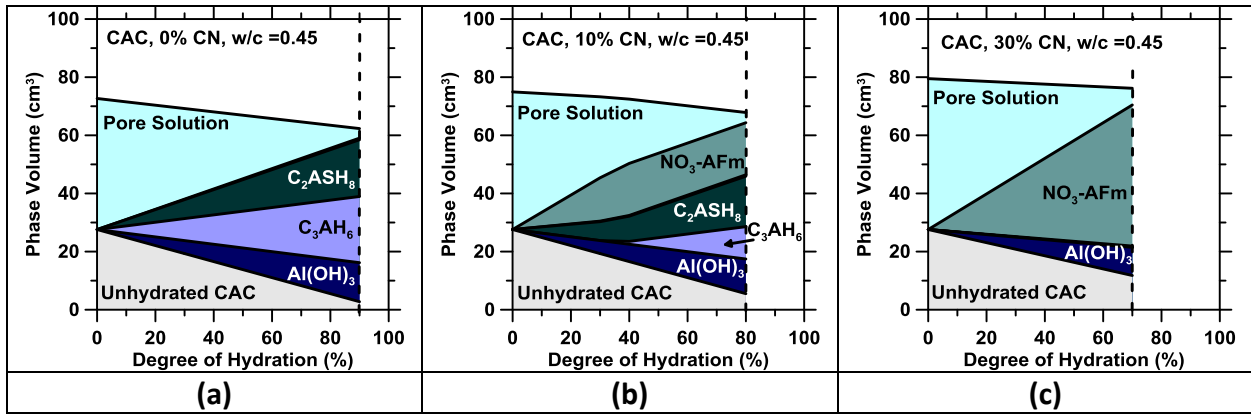


Figure 1: The hydrated phase assemblages calculated using GEMS for CAC systems for $w/c = 0.45$ containing: (a) 0 mass % CN, (b) 10 mass % CN, and (c) 30 mass % CN [28]. These calculations consider 100 g of anhydrous CAC reacting with 45 g of water/CN solution. The dashed vertical line shows the maximum simulated degree of hydration for each system. At a degree of hydration greater than this value, chemical reactions will cease due to limitations on water availability.

255
 256 **3.2 Cl^- binding isotherms**
 257 Figure 2 shows the free Cl^- concentration, $C_{Cl,f}$ as a function of time from 0 to 21 d. The solution
 258 concentrations are seen to stabilize by 21 d wherein the relative difference in Cl^- concentrations
 259 at 21 d and the previous measurement was $\leq 5\%$ (i.e., within the measurement resolution). Thus,
 260 the measured free Cl^- concentrations at 21 d were used to calculate the bound Cl^- content (i.e.,
 261 expressed in terms of moles of Cl^- bound per kg of hydrated CAC paste) as:

$$C_{Cl,b}^{eq} = \frac{(C_{Cl,f}^0 - C_{Cl,f}^{21}) \cdot V_{sol}}{m_{paste}} \quad (2)$$

262
 263 where, $C_{Cl,f}^0$ and $C_{Cl,f}^{21}$ represent the concentrations of free Cl^- in solution (in terms of mol Cl^- per
 264 L of solution) measured initially, and after 21 d of immersion (t near-equilibrium), respectively.
 265

266 Figure 3 shows the equilibrium Cl^- binding isotherms for each hydrated CAC paste. The bound Cl^-
 267 content is substantially larger for CN-dosed CAC pastes for CN dosage levels ≥ 10 mass %. As
 268 expected, the isotherms are non-linear, and demonstrate a plateau in binding at higher Cl^-
 269 concentrations. The binding isotherms can be described by a Langmuir expression as [71]:

$$C_{Cl,b}^{eq}(C_{Cl,f}) = \frac{\alpha \cdot C_{Cl,f}}{1 + \beta \cdot C_{Cl,f}} \quad (3)$$

271 where, $C_{Cl,b}^{eq}$ is the equilibrium bound Cl^- concentration (mol Cl^- / kg CAC paste), $C_{Cl,f}$ is the free Cl^-
 272 concentration in solution at equilibrium (mol Cl^- /L solution), and α (L solution/kg CAC paste) and
 273 β (L solution/mol Cl^-) are fitting parameters (see Table 2) [46,72]. As a point of comparison, it
 274 should be noted that the Cl^- binding capacity of a typical “neat-OPC” system is approximately
 275 25 % that of the “neat CAC” system shown in Figure 3; at a similar w/c and temperature [32].
 276

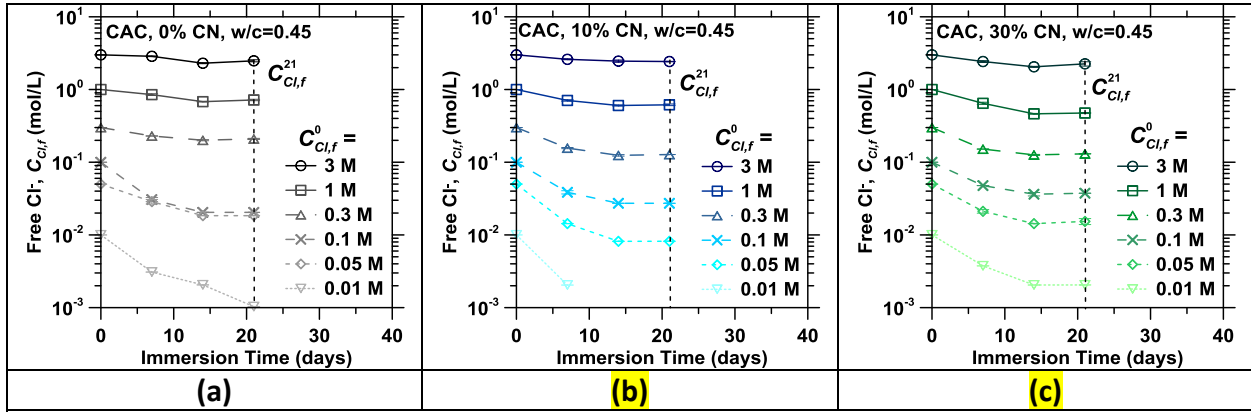


Figure 2: The free Cl^- concentration ($C_{Cl,f}$) in solution as a function of time for $CaCl_2 \cdot 2H_2O$ solutions in contact with hydrated CAC pastes containing: (a) 0 mass % CN, (b) 10 mass % CN, and (c) 30 mass % CN over the concentration range: $0.01 \text{ mol/L} \leq C_{Cl,f}^0 \leq 3 \text{ mol/L}$. The coefficient of variation of the $C_{Cl,f}$ measurements was $\approx 5\%$.

277

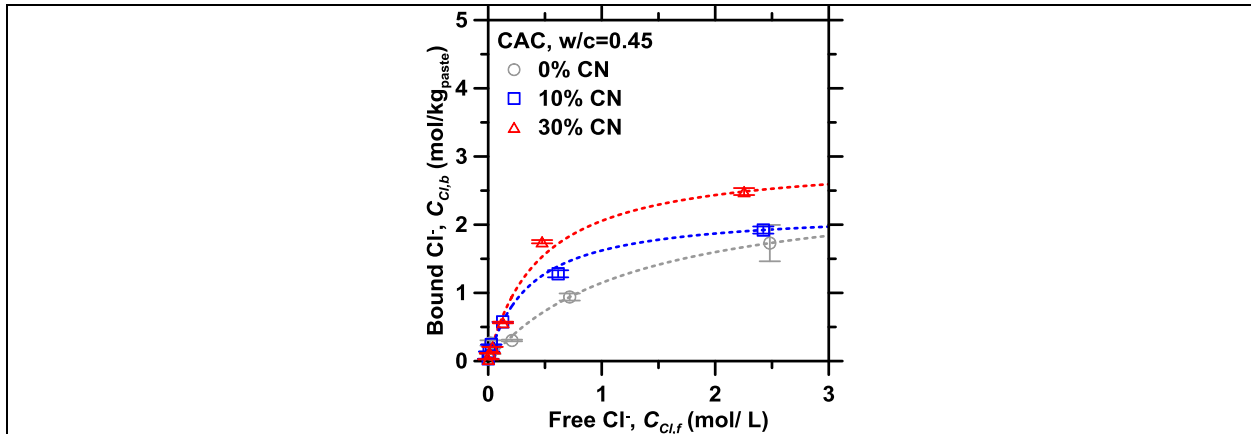


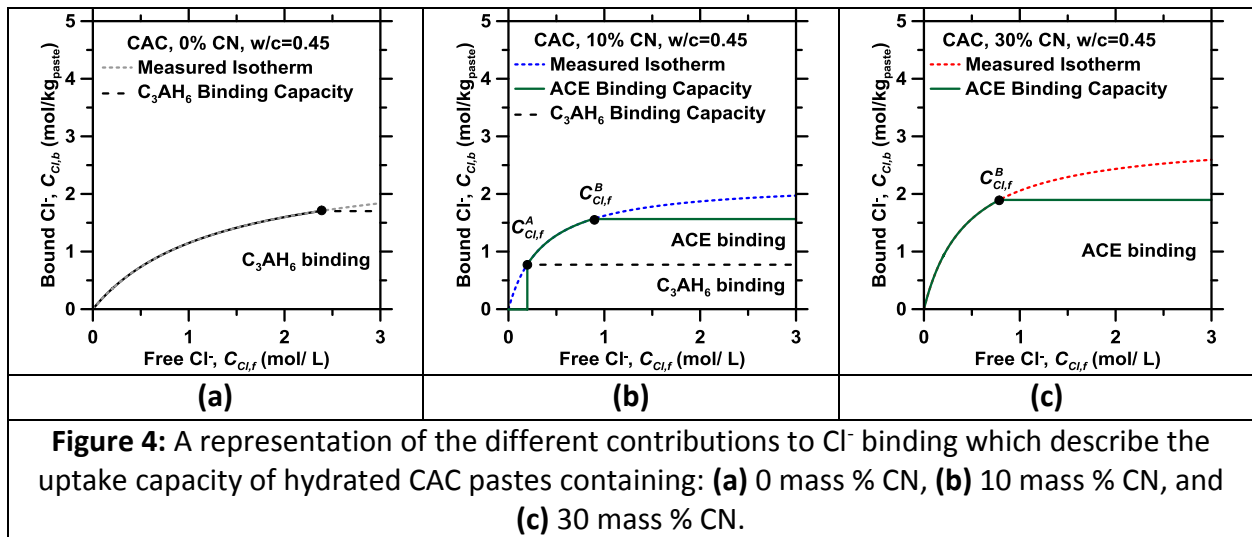
Figure 3: The measured Cl^- binding isotherms for the hydrated CAC pastes following 21 d of immersion in $CaCl_2 \cdot 2H_2O$ solutions. The error bars indicate \pm one standard deviation in the experimental measurements, which were performed in triplicate.

278

279 To better explain the measured Cl^- binding isotherms, the phase assemblages calculated using
 280 GEMS were used to estimate the binding capacity of the CAC pastes. Assuming the destabilization
 281 of 1 unit of C_3AH_6 (i.e., which occurs at $\approx 0.01 \text{ mol } Cl^-/L$ [29]) allows the incorporation of 2 units
 282 of Cl^- to form Friedel’s salt ($C_3A \cdot CaCl_2 \cdot H_{10}$), C_3AH_6 features a Cl^- binding capacity of $5.36 \text{ mol } Cl^-/kg$
 283 C_3AH_6 . This binding capacity is greater than that resulting from the uptake of Cl^- into NO_3^- -AFm
 284 ($3.10 \text{ mol } Cl^-/kg \text{ } NO_3^-$ -AFm). This explains why the 0 mass % CN and 10 mass % CN mixtures show

285 similar binding isotherms. But, increasing the CN dosage enhances Cl^- binding in spite of reducing
 286 the quantity of C_3AH_6 present by suppressing the formation of C_2ASH_8 (which is not expected to
 287 bind Cl^- ions) while enhancing the quantity of NO_3^- -AFm that is formed; wherein the latter shows
 288 significant Cl^- binding by ion exchange.

289
 290 To discriminate the effects of Cl^- binding via ACE, which releases NO_3^- ions, and binding via C_3AH_6
 291 destabilization (i.e., which does not result in NO_3^- release), the Cl^- binding capacity of each CAC
 292 formulation was calculated as the mass-average based on its thermodynamically modeled phase
 293 assemblage, and while assuming complete conversion of C_3AH_6 to Friedel's salt. Figure 4 shows
 294 the calculated Cl^- binding contributions for each CAC paste overlaid onto its respective Cl^- binding
 295 isotherm. The majority of the Cl^- binding isotherm of each CAC paste is explained by its binding
 296 capacity calculated based on its predicted phase assemblage. The difference in the measured and
 297 calculated isotherms is thought to arise from discrepancies between the thermodynamically
 298 modeled phase assemblages and those of the "real" experimental system. However, seeing that
 299 this difference increases with CN dosage (i.e., or rather, the quantity of unreacted CAC present;
 300 see Figure 3), it is postulated that the difference dominantly results from the reaction between
 301 unreacted CAC with Cl^- in solution, and physisorption of Cl^- species onto the residual hydrated
 302 phases (e.g., C_2ASH_8). Assuming that C_3AH_6 converts to Cl -AFm before Cl -for- NO_3 exchange by the
 303 AFm initiates, the influence of ACE binding can be modeled by a multi-step function. This function
 304 equals zero below a critical concentration of free Cl^- , following which it traces the Cl^- binding
 305 isotherm. As confirmed by Puerta-Falla et al., Cl -for- NO_3 exchange is set to be equivalent (i.e., to
 306 ensure 1:1 monovalent ion exchange) to satisfy conditions of electroneutrality in solution [73].
 307



308
 309 **3.2 Electrical impedance spectroscopy**
 310 The EIS response (i.e., a Nyquist plot) of a representative CAC mortar ($\phi_q = 0.50$) for different CN
 311 dosages is shown in Figure 5(a). The bulk resistance was quantified as the real component of
 312 impedance (Z') at which the imaginary impedance (Z'') displayed a minimum. The bulk electrical
 313 conductivity (σ_{eff} , S/m) of the hydrated specimens was calculated as (see Section 2.2.4):

$$314 \quad \sigma_{eff} = k/R_b \quad (4)$$

315 Figure 5(b) shows the effective conductivity of CAC mortars as a function of quartz sand volume
 316 fraction. At a given quartz volume fraction, the effective conductivity decreases as the CN dosage
 317 increases from 0 mass % to 10 mass % CN, and then increases dramatically at the 30 mass % CN
 318 dosage. This conductivity minimum is thought to be produced on account of alterations in pore
 319 structure/connectivity due to the changes in phase assemblages, although this aspect requires
 320 further study. In each case, the bulk conductivity decreases as the volume fraction of quartz sand
 321 increases. This is due to dilution of the porous CAC paste matrix, and the reduction in its
 322 connectivity (i.e., an increase in tortuosity) due to the presence of non-porous (sand) inclusions
 323 [74,75]. This trend is opposite to that observed in OPC mortars, in which ionic diffusivity increases
 324 when aggregates are present due to the percolation of the porous interfacial transition zones
 325 (ITZ) between the aggregates [74,75]. The values of D_i^{inf} for ions pertinent to seawater are listed
 326 in Table 1. The calculated values of σ_0 and the factor σ_{eff}/σ_0 for each cementitious composition
 327 are given in Table 2. As a point of reference it should be noted that the CAC mortars feature ionic
 328 diffusion coefficients that are equivalent to, or approximately one order of magnitude less than
 329 that of a typical OPC concrete [76].
 330

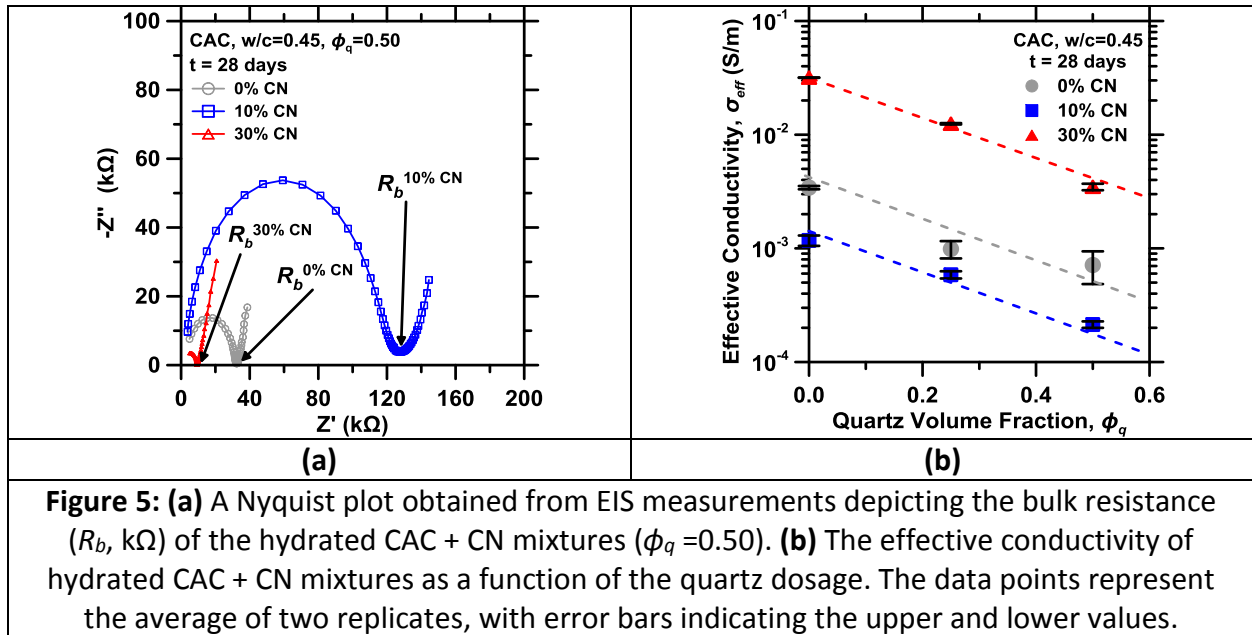


Figure 5: (a) A Nyquist plot obtained from EIS measurements depicting the bulk resistance (R_b , k Ω) of the hydrated CAC + CN mixtures ($\phi_q=0.50$). (b) The effective conductivity of hydrated CAC + CN mixtures as a function of the quartz dosage. The data points represent the average of two replicates, with error bars indicating the upper and lower values.

331
 332
 333
 334
 335
 336
 337
 338
 339
 340

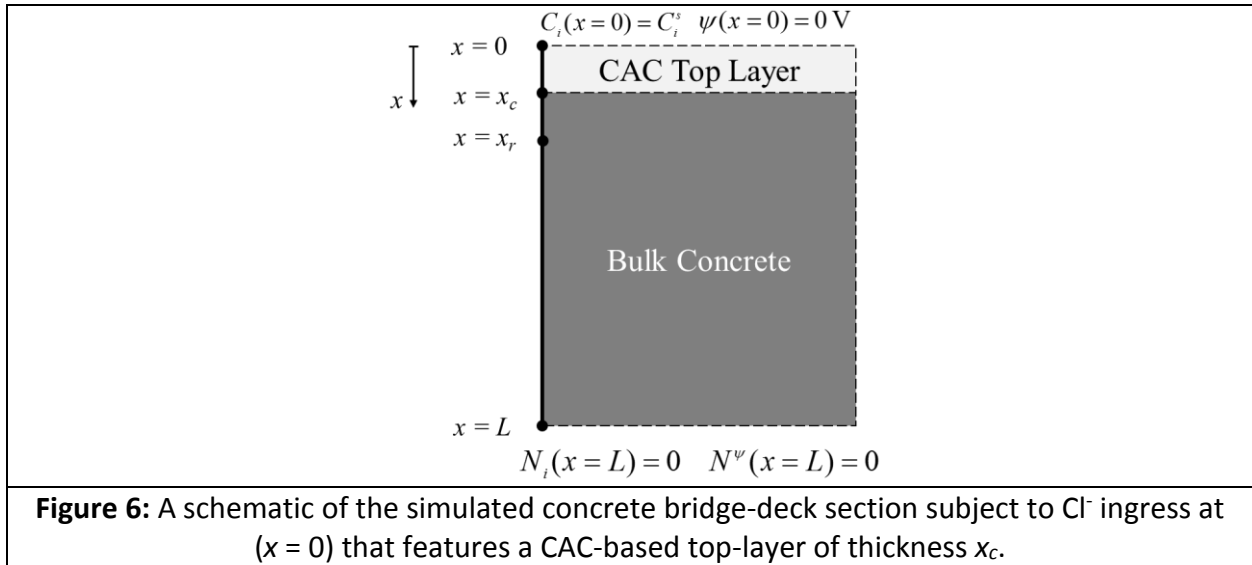
4. Formulation of multispecies reaction-transport model

4.1 Schematic and assumptions

To elucidate the benefits of ACE, a simplified concrete bridge-deck geometry (also representative of a pier with one-face exposed to seawater) was developed. This 1D-domain of a pristine (i.e., uncracked) concrete section is shown in Figure 6. The concrete section has a thickness of $L = 0.2$ m, a fraction of which comprises a CAC-based top-layer of thickness $x_c = 0.025$ m. The depth of the reinforcing steel from the upper surface (i.e., the cover depth) is assumed to be $x_r = 0.050$ m. To describe ion transport, the following assumptions were made:

- The porosity of the concrete and the CAC-based top-layers is saturated with pore solution,

- 341 • Advective transport of ions is negligible as a zero pressure gradient is assumed in the pores,
342 hence the pore solution velocity (and Péclet number) is zero, assuming no moisture transport
343 is induced by cyclic wetting-and-drying [43,77],
- 344 • The effects of ion-activity (i.e., non-ideality of the solution) on transport are not accounted
345 for since this factor exerts second order contributions to the transport response [78,79],
- 346 • The effects of electrical coupling between ions is significant enough to warrant multispecies
347 modeling [42,80], and,
- 348 • The electrical double layer present on the hydrated solids does not affect transport [81], since
349 ion transport takes place dominantly through larger capillary pores which remain percolated,
350 rather than through the nanoscale gel pores, e.g., as present in the C-S-H [68].
351



352
353 **4.2 Governing equations**
354 For the assumptions noted above, the concentrations of multiple ionic species in solution as a
355 function of space (x) and time (t) can be described by the Nernst-Planck (NP) equation:

356
$$\frac{\partial C_{i,f}}{\partial t} + \frac{\partial}{\partial x} \cdot \left(-D_i \frac{\partial C_{i,f}}{\partial x} - z_i \frac{D_i}{RT} F C_{i,f} \cdot \frac{\partial \psi}{\partial x} \right) = v_i \quad (5)$$

357 where, $C_{i,f}$ is the free concentration of the i^{th} species within the pore solution (mol/L), D_i is the
358 diffusion coefficient of the i^{th} ionic species within the relevant cementitious matrix (m^2/s), z_i is
359 the valence of the i^{th} species, R is the universal gas constant ($8.314 \text{ J/mol}\cdot\text{K}$), T is the temperature
360 (K), F is Faraday's constant (96484.56 C/mol), ψ is the electric potential (V), and v_i is the reaction
361 rate of the i^{th} species ($\text{mol}/(\text{L}\cdot\text{s})$). The NP equation is governed by the ionic concentrations of n -
362 1 species, where n is the total number of ionic species considered. The concentration of the final
363 (n^{th}) species is governed by the electroneutrality assumption (i.e., zero charge density) which is a
364 simplification of the Poisson equation [82]:

365
$$\sum_i z_i C_{i,f} = 0 \quad (6)$$

366 The reaction rate (v_i) in Equation (5) for all species except Cl^- and NO_3^- was assumed to be zero
 367 (i.e., no reaction between species). The reaction rates corresponding to the Cl^- and NO_3^- species
 368 are expressed by the following first order reactions:

$$369 \quad v_{\text{Cl}} = k_{\text{Cl}} \left(C_{\text{Cl},b} - C_{\text{Cl},b}^{\text{eq}}(C_{\text{Cl},f}) \right) \quad (7)$$

$$370 \quad v_{\text{NO}_3} = -k_{\text{Cl}} \left(C_{\text{NO}_3}^{\text{max}} - C_{\text{NO}_3}^{\text{eq}}(C_{\text{Cl},f}) \right) \quad (8)$$

371 where, k_{Cl} is the reaction rate constant of Cl-for- NO_3^- ion exchange (s^{-1}), and $C_{\text{NO}_3}^{\text{max}}$ is the maximum
 372 NO_3^- concentration predicted in the pore solution upon exhaustion of the system's ACE capacity.
 373 Since Cl⁻ for NO_3^- exchange in AFm is stoichiometric (i.e., 1 mol Cl^- replaces 1 mol NO_3^-), the molar
 374 fluxes of these species are equal and opposite when ACE is the means of Cl^- binding [73]. The Cl^-
 375 binding isotherm $C_{\text{Cl},b}^{\text{eq}}(C_{\text{Cl},f})$ for any cementitious formulation is given by the Langmuir isotherm
 376 parameters noted in Figure 3, scaled to the appropriate units by the paste content and porosity
 377 given in Table 2. The binding response, i.e., including the effects of C_3AH_6 conversion, Cl^- -for- NO_3^-
 378 exchange and the hydration of residual CAC, if any, is given by a piecewise function written as:

$$379 \quad C_{\text{NO}_3}^{\text{eq}}(C_{\text{Cl},f}) = \left\{ \begin{array}{ll} 0, & 0 \text{ mol/L} \leq C_{\text{Cl},f} \leq C_{\text{Cl},f}^{\text{A}} \\ \frac{\alpha \cdot C_{\text{Cl},f}}{1 + \beta \cdot C_{\text{Cl},f}}, & C_{\text{Cl},f}^{\text{A}} \leq C_{\text{Cl},f} \leq C_{\text{Cl},f}^{\text{B}} \\ C_{\text{NO}_3}^{\text{max}}, & C_{\text{Cl},f}^{\text{B}} \leq C_{\text{Cl},f} \end{array} \right\} \quad (9)$$

380 where, $C_{\text{Cl},f}^{\text{A}}$ and $C_{\text{Cl},f}^{\text{B}}$ are the free Cl^- concentrations at which binding by ACE begins, and ends,
 381 respectively. Cl^- binding was modeled as a first-order reaction, in which the driving force is given
 382 simply by the difference between the currently bound Cl^- content, and the equilibrium bound Cl^-
 383 content predicted by the relevant (mixture dependent) binding isotherm shown in Figure 3. Thus,
 384 the following equation was solved for $C_{\text{Cl},b}$:

$$385 \quad \frac{dC_{\text{Cl},b}}{dt} = k_{\text{Cl}} \left(C_{\text{Cl},b} - C_{\text{Cl},b}^{\text{eq}}(C_{\text{Cl},f}) \right) \quad (10)$$

386

387 **4.3 Initial and boundary conditions**

388 The concentrations of ions at the exposed surface (i.e., $x = 0$) was set to conform with those of
 389 seawater [83]; as noted in Table 1. Table 1 also details the concentrations of ions in the pore
 390 solution of the OPC and CAC formulations. The compositions of pore solutions were estimated
 391 by thermodynamic calculations (for the CAC formulations) or sourced from the literature (for the
 392 OPC system). As expected, the CN-dosed CAC systems show large concentrations of NO_3^- species
 393 in their pore solutions, and a pH (OH^- abundance) that is lower than an OPC-concrete system [84].
 394

395 Assuming ions cannot escape the bottom of the bridge-deck (e.g., due to the presence of stay-
 396 in-place metal forms), a zero-flux boundary condition is imposed at $x = L$:

$$397 \quad N_i(x = L) = - \left(D_i \frac{\partial C_i}{\partial x} - z_i \frac{D_i}{RT} F C_i \cdot \frac{\partial \psi}{\partial x} \right) = 0 \quad (11a)$$

398 where, N is the flux of the i^{th} ionic species ($\text{mol}/\text{m}^2 \cdot \text{s}$). Additionally, this lack of "ion escape" also
 399 implies electrical insulation (i.e., zero current) at the same boundary:

400
$$N^w(x=L) = F \sum_i z_i \left(-D_i \frac{\partial C_i}{\partial x} - z_i \frac{D_i}{RT} F C_i \cdot \frac{\partial \psi}{\partial x} \right) = 0 \quad (11b)$$

401 where, N^w is the electrical current density (A/m²). The potential at the exposed surface of the
 402 concrete bridge deck was assumed to be zero, i.e., grounded:

403
$$\psi(x=0) = 0 \text{ V} \quad (12)$$

404 A perfect bond was assumed between the CAC top-layer and the bulk OPC concrete, and no
 405 buildup of electric charge was assumed at the interface. Therefore, ionic flux and electric current
 406 density were assumed to be continuous across the interface ($x = L_c$).
 407

Table 1: The ion-dependent diffusion coefficients at infinite dilution (D_i^{inf}) at $T = 25 \text{ }^\circ\text{C}$ [85], the boundary conditions (i.e., concentrations of each ionic species at the exposed surface; $x = 0 \text{ m}$, with C_i^s corresponding to seawater [83]), and the initial conditions of the simulations (i.e., the concentrations of ions within the pore solution of each cementitious matrix).

Ionic Species	D_i^{inf} ($10^{-9} \text{ m}^2/\text{s}$)	C_i^s (mmol/L)	$C_i^{0\% \text{ CN}}$ (mmol/L)	$C_i^{10\% \text{ CN}}$ (mmol/L)	$C_i^{30\% \text{ CN}}$ (mmol/L)	$C_i^{\text{OPC}^*}$ (mmol/L)
Na ⁺	1.33	480	0	0	0	140
K ⁺	1.96	10	0	0	0	210
Ca ²⁺	0.793	10	23.1	23.2	57.1	0
Mg ²⁺	0.705	53	0	0	0	0
Al(OH) ₄ ⁻	1.04	0	20.0	20.0	20.0	0
OH ⁻	5.27	0.0013	26.1	24.5	7.8	330
Cl ⁻	2.03	560	0	0	0	0
NO ₃ ⁻	1.90	0	0	1.9	86.3	0
SO ₄ ²⁻	1.07	29	0	0	0	10

(*) Aguayo et al. [86]

408

Table 2: The material-specific input parameters representing: Cl⁻ binding, formation factor (i.e., which dictates ion diffusion rates within a constrained microstructure), and the mixture compositions (i.e., the porosity and paste content of the CAC mortars and OPC concrete).

Material	α (L / kg _{paste})	β (L / mol Cl ⁻)	Binding rate constant, k_{Cl} (s ⁻¹)	σ_{eff} / σ_0	Porosity (φ_p)	Paste content (kg / m ³ concrete)
CAC + 0% CN	0.00204	0.00077	1×10^{-7}	1.14×10^{-3}	0.14	870
CAC + 10% CN	0.00608	0.00275	1×10^{-7}	3.50×10^{-4}	0.09	970
CAC + 30% CN	0.00661	0.00222	1×10^{-7}	3.68×10^{-3}	0.06	1020
OPC Concrete	0.00352*	0.00416*	1×10^{-7}	$4.0 \times 10^{-3}^\dagger$	0.11 [‡]	920

(*) Dhir et al. [32], (†) Bentz et al. [76], (‡) Birdsall et al. [87].

409 Table 2 displays additional material-specific parameters used in the simulations. These include
410 the Langmuir isotherm parameters and reaction rate constants, the factor σ_{eff}/σ_0 , porosity and
411 paste content. The maximum uncertainties in α and β were ± 0.0005 , and ± 0.0001 , respectively.
412 The porosity of each CAC composition was calculated – from its volumetric phase assemblage at
413 a degree of reaction of 70 % – as the fractional volume of the liquid phase present in the system
414 [88]. Although the binding rate constant of Cl^- for NO_3^- exchange in AFm's has been measured to
415 be on the order of $[1.0 \pm 0.2] \times 10^{-5} \text{ s}^{-1}$, to improve numerical convergence, the rate constant was
416 estimated as $1 \times 10^{-7} \text{ s}^{-1}$ across all compositions [73]. This reduction however, does not
417 significantly influence the results, as the process remains diffusion-limited (i.e., with Damköhler
418 number $\gg 1$) and binding can be approximated as instantaneous. Indeed, over simulated time
419 scales of 1-to-100 years, the simulated Cl^- and NO_3^- concentrations vary by $<1\%$ at any x as the
420 binding rate constant is increased (not shown).

421

422 **4.4 Method of solution**

423 The governing equations (Equations 5 to 10) were solved using the specific initial and boundary
424 conditions (Equations 11-12 and Table 1) within COMSOL Multiphysics 4.3¹, a commercial finite
425 element solver, using the “Chemical Reaction Engineering Module”. Numerical convergence was
426 considered to be reached when the highest relative difference in Cl^- concentration profiles was
427 $\pm 1\%$, when reducing the element size or time step by a factor of 2. In practice, converged
428 solutions were obtained by imposing a maximum time step of $1 \times 10^5 \text{ s}$, while using the adaptive
429 time-stepping algorithm built-in to COMSOL and a fixed element size of $5 \times 10^{-4} \text{ m}$.

430

431 **5. Results of finite element simulations**

432 **5.1 Cl^- transport from seawater**

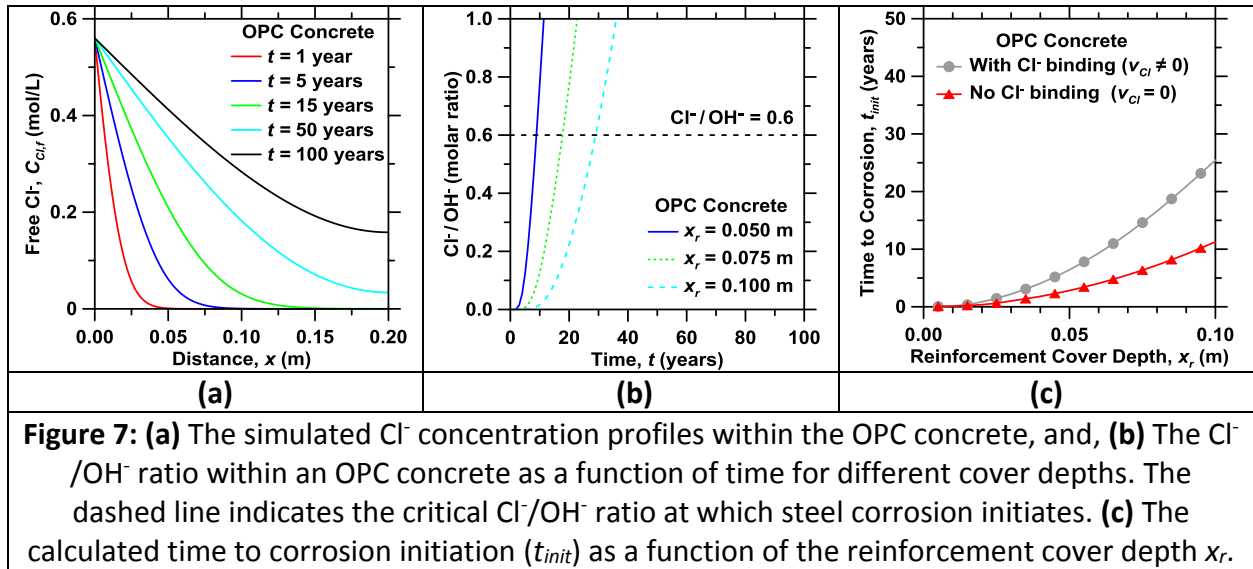
433 The first set of simulations considered surface exposure of an OPC bridge-deck to seawater, the
434 concentration and volume of which remain fixed. Figure 7(a) shows simulated Cl^- concentration
435 profiles within a neat-OPC concrete as a function of distance, x , from the exposed surface. As
436 expected, Cl^- concentrations rise dramatically through the depth of the concrete over time. The
437 corresponding Cl^-/OH^- ratio at various depths in the cover-zone typical for bridge-decks is shown
438 in Figure 7(b).

439

440 It is seen that Cl^-/OH^- ratios exceed 0.6 within 30 years; i.e., which would assure corrosion
441 initiation and its progression. Conservatively, the service life of the bridge-deck is defined by the
442 time interval prior to corrosion initiation (t_{init}); i.e., the period in which $\text{Cl}^-/\text{OH}^- \leq 0.6$. For an OPC
443 cover depth $x_r = 0.050 \text{ m}$, that is typical for bridge decks, corrosion is expected to initiate for t_{init}
444 = 6.4 years. Obviously, increasing the cover depth above steel reinforcement (x_r) to 0.075 m or
445 0.100 m delays t_{init} to 14.6 years or 25.5 years, respectively. Figure 7(c) displays t_{init} as a function
446 of x_r within an OPC concrete bridge-deck. The influence of Cl^- binding within the OPC concrete is
447 significant, as a result of which t_{init} approximately doubles for $x_r \geq 0.025 \text{ m}$. While increasing the
448 cover depth does delay the onset of corrosion, this is often considered as an inefficient and cost-
449 prohibitive mitigation approach.

450

451



452

453 Second, a scenario was simulated wherein the top 0.025 m of OPC concrete was replaced with a
 454 plain CAC mortar top-layer. Figure 8(a) displays Cl^- concentration profiles for such a bridge-deck,
 455 wherein the mortar (CAC + 0 % CN) contains a quartz inclusion volume fraction, $\phi_q = 0.50$. In this
 456 case, the combined effects of lower ionic diffusivity ($\approx \frac{1}{4}$ that of OPC concrete) and enhanced Cl^-
 457 binding of the CAC top-layer retard Cl^- ingress relative to the OPC concrete (i.e., by increasing t_{init}
 458 from 6.4 years to 28.5 years). To highlight these effects on t_{init} , detailed simulations were carried
 459 out while assuming: (i) the Cl^- binding capacity of the CAC paste to be similar to the OPC system
 460 ($\text{Bind}_{top} = \text{Bind}_{bulk}$), and, (ii) the ion-diffusivity of the CAC mortar is equivalent to that of the OPC
 461 concrete ($D_{top} = D_{bulk}$). The resulting Cl^-/OH^- ratios are displayed in Figure 8(b) for a fixed cover
 462 depth, $x_r = 0.050$ m. The reduced ionic diffusivity of the CAC mortar is identified as the primary
 463 cause of an increased time to corrosion initiation, as $t_{init} = 18.4$ years solely on the account of
 464 retarded ion diffusion (case i, $\text{Bind}_{top} = \text{Bind}_{bulk}$), while $t_{init} = 9.1$ years when only an increase in Cl^-
 465 binding capacity is considered (case ii, $D_{top} = D_{bulk}$). Nevertheless, the effects of enhanced Cl^-
 466 binding are significant. When the effects of enhanced binding are negated (i.e., by setting Bind_{top}
 467 = Bind_{bulk}), Cl^- concentrations in solution are greater as compared to when enhanced binding and
 468 reduced diffusivity function in tandem. This clearly indicates the potential benefits of enhanced
 469 Cl^- binding in increasing service life.

470

471 To further compare the efficacy of CAC top-layers in corrosion mitigation, a corrosion delay factor
 472 (d_f) was defined as $d_f = t_{init}(\text{CAC})/t_{init}(\text{OPC concrete})$. Figure 8(c) displays the corrosion delay factor
 473 as a function of the reinforcement cover depth in the 0 % CN CAC case. In each case, the corrosion
 474 delay factor shows a maximum for $0.01 \text{ m} \leq x_r \leq 0.03 \text{ m}$, illustrating an optimal efficacy of the CAC
 475 top-layer thickness relative to the depth of reinforcing steel. Maximum delay factors range from
 476 2.9 to 13.9, depending on the parameters imposed. It should be noted that these outcomes are
 477 broadly independent of the critical Cl^-/OH^- ratio at which corrosion initiates. This is because the
 478 critical Cl^-/OH^- ratio influences the magnitude of t_{init} , but only weakly affects d_f .

479

480

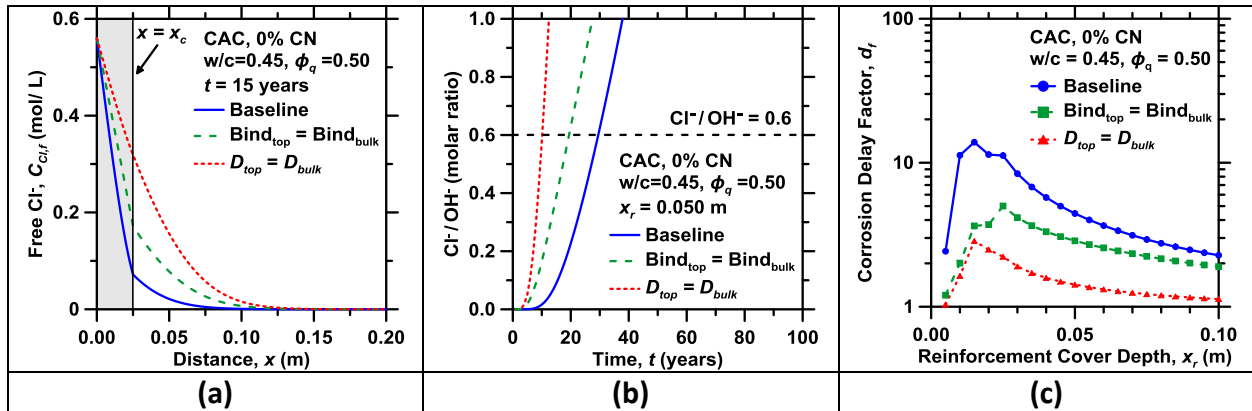


Figure 8: (a) The simulated Cl⁻ concentration profiles within an OPC concrete topped with a 0 mass % CN CAC top-layer ($\phi_q = 0.50$, $x_c = 0.025$ m) after 15 years of exposure to seawater. The dashed lines show scenarios wherein a Cl⁻ binding isotherm equal to that of the OPC paste was assumed in the CAC top-layer ($\text{Bind}_{\text{top}} = \text{Bind}_{\text{bulk}}$), or, wherein the CAC top-layer and the OPC concrete are assumed to have similar ionic diffusivities ($D_{\text{top}} = D_{\text{bulk}}$). (b) The Cl⁻/OH⁻ ratio as a function of time at a cover depth $x_r = 0.050$ m. The horizontal dashed line in (b) indicates the critical Cl⁻/OH⁻ ratio when steel corrosion initiates. (c) The corrosion delay factor (d_f) produced by replacement of the OPC concrete with a 0 mass % CN CAC top-layer, as a function of reinforcement cover depth x_r .

481

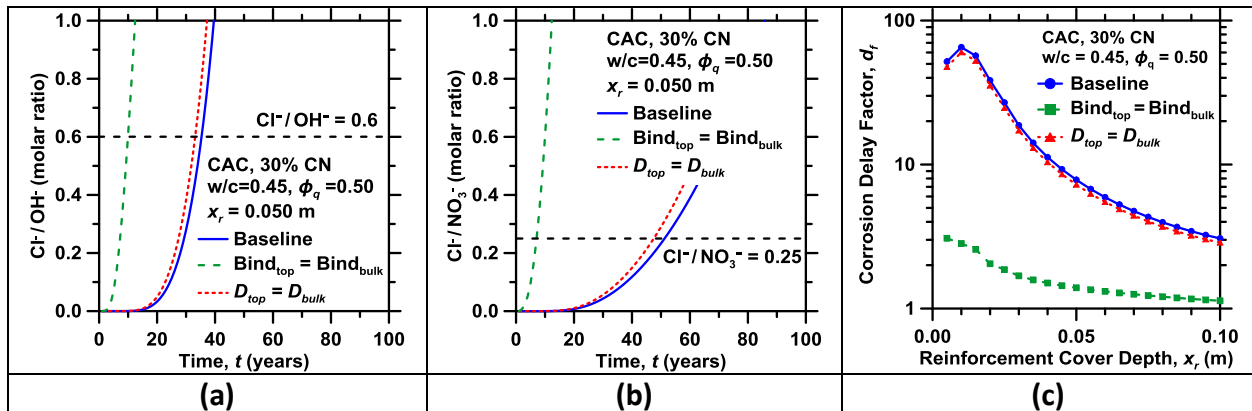


Figure 9: (a) The Cl⁻/OH⁻ ratio, and, (b) The Cl⁻/NO₃⁻ ratio within OPC concrete topped with a 30 mass % CN CAC top-layer ($\phi_q = 0.50$, $x_c = 0.025$ m) as a function of time for a cover depth $x_r = 0.050$ m. The horizontal dashed lines in (a) and (b) indicate the critical Cl⁻/OH⁻ and Cl⁻/NO₃⁻ ratios for the initiation of steel corrosion or inability for the re-passivation of steel by NO₃⁻. (c) The corrosion delay factor (d_f) produced by replacing OPC concrete with a 30 mass % CN CAC top-layer, as a function of reinforcement cover depth x_r .

482

483 The effects of CN additions to CAC's were also investigated. Figure 9(a) shows calculated Cl⁻/OH⁻
 484 ratios at $x_r = 0.050$ m when an OPC-concrete is topped with a CAC top-layer dosed with 30 mass
 485 % CN. The coupled effects of (very slightly) reduced ion-diffusion and substantially enhanced Cl⁻
 486 binding dramatically hinders Cl⁻ transport in comparison to OPC concrete. In fact, the 30 % CN
 487 composition shows a greater delay efficacy than the 0 % CN composition, despite the fact that its
 488 ionic diffusivity is 3x higher. This indicates that the benefits of amplified Cl⁻ binding capacity of

489 the 30 % CN system far outweighs its increased diffusivity. Unlike the 0 mass % CN case, in which
 490 the ion-diffusivity reduction plays a prominent role, enhanced Cl^- capture and the associated NO_3^-
 491 exchange are observed to be the dominant mechanisms of corrosion delay. Due to the similarity
 492 of the diffusivity within the CAC mortar and OPC concrete, when Cl^- binding within the CAC top-
 493 layer is equated to that of OPC (Figure 9a, $\text{Bind}_{\text{top}} = \text{Bind}_{\text{bulk}}$); Cl^- ingress is only slightly reduced,
 494 resulting in a predicted time to corrosion of $t_{\text{init}} = 8.9$ years at a cover depth $x_r = 0.050$ m (i.e.,
 495 when $\text{Cl}^-/\text{OH}^- \leq 0.60$). However, due to the high initial NO_3^- concentration in the pore solution,
 496 and NO_3^- exchange enabled by the NO_3^- -AFm, the time to corrosion is expected to be extended.
 497

498 For clarity, Figure 9(b) displays the relevant $\text{Cl}^-/\text{NO}_3^-$ ratios as a function of time. When both ionic
 499 diffusivity and binding effects are considered, the presence of NO_3^- in the pore solution extends
 500 t_{init} to 50.2 years (i.e., when $\text{Cl}^-/\text{NO}_3^- \geq 0.25$). But, when Cl^- binding is equivalent to the OPC system
 501 (i.e., $\text{Bind}_{\text{top}} = \text{Bind}_{\text{bulk}}$), $\text{Cl}^-/\text{NO}_3^-$ quickly exceeds the critical passivation ratio resulting in corrosion
 502 initiation. In this case, the presence of NO_3^- does not improve service life, as the time period when
 503 $\text{Cl}^-/\text{NO}_3^- \leq 0.25$ is less than that at which $\text{Cl}^-/\text{OH}^- \leq 0.6$. These findings are supported by the
 504 significant increase in the corrosion delay factor (e.g., see Figure 9c) which exceeds 65 due to the
 505 combined effects of reduced diffusivity and enhanced ACE, as compared to only 3 when the
 506 effects of enhanced ACE are neglected.
 507

508 **5.2 Parametric study**

509 To deconvolute the effects of enhanced Cl^- binding, reduced ionic diffusivity, and of NO_3^- release
 510 (i.e., simultaneous anion capture and exchange) on the time to corrosion initiation, a parametric
 511 study was carried out. The simulations considered CAC top-layers with 0 %, 10 %, and 30 % by
 512 mass CN, with binding isotherms corresponding to Figure 3; but with an ionic diffusivity equal to
 513 that of the OPC concrete. Figure 10(a) displays the corrosion delay factor (d_f) that is predicted for
 514 these conditions as a function of the fraction of cover depth composed of CAC (x_c/x_r); for a cover
 515 depth $x_r = 0.050$ m. To set the performance of the baseline scenario, the time to steel corrosion
 516 initiation for the OPC concrete system is determined to be 6.4 years.
 517

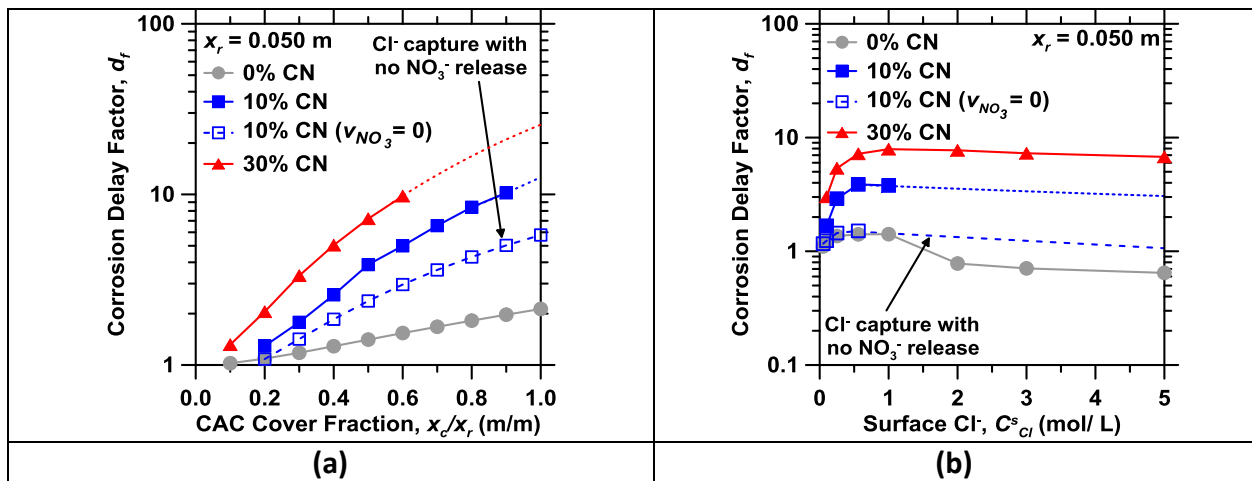


Figure 10: The corrosion delay factor relative to OPC concrete as a function of: (a) The fractional thickness of the CAC top-layer (x_c/x_r), and (b) The surface Cl^- concentration (C_{Cl}^s), for a reinforcement cover depth $x_r = 0.050$ m.

518 For all CAC compositions, increasing the CAC layer thickness increases the time to steel corrosion
519 initiation, resulting in corrosion delay factors > 1 . For example, when 0.050 m of OPC cover is
520 replaced by a 0 mass % CN CAC mortar top-layer, the time to corrosion initiation doubles. As the
521 CN dosage increases, the provision of CAC top-layers increasingly extends the time to steel
522 corrosion initiation. This is largely due to the release of the NO_3^- ions via ACE ensuring that the
523 $\text{Cl}^-/\text{NO}_3^- \leq 0.25$. To carefully illustrate the benefits of NO_3^- release in the CAC + 10 mass % CN top-
524 layer, the NO_3^- reaction rate (i.e., $v_{\text{NO}_3^-}$, Equation 8) was set to zero. In this case, due to the
525 insufficient concentration of free NO_3^- in the pore solution, the service life predicted by the Cl^-
526 $/\text{OH}^-$ ratio exceeds that predicted by the critical $\text{Cl}^-/\text{NO}_3^-$ ratio. However, due to enhanced Cl^-
527 binding, the time to achieve the critical Cl^-/OH^- ratio (Figure 10) is significantly extended relative
528 to the OPC concrete. Despite the similarity between their Cl^- binding isotherms, the CAC + 10
529 mass % CN top-layer demonstrates larger delay factors than the 0 mass % CN CAC mortar top-
530 layer. This can be attributed to the lower porosity and the higher paste content in the CAC + 10
531 mass % CN system, which increases the amount of CAC paste available for Cl^- capture from the
532 pore solution. While the effects of enhanced Cl^- capture in this system are substantial, the
533 corrosion delay factor is only one-half of that when ACE (NO_3^- release) is considered.

534
535 To examine the benefits of ACE over a wider range of surface Cl^- concentrations, i.e., beyond just
536 seawater exposure, a broader set of simulations were carried out. Here, electroneutrality in the
537 solution at the surface was maintained by modifying the Na^+ concentration concurrently with
538 that of Cl^- (i.e., assuming NaCl as the Cl^- source) – and the thickness of the CAC top-layer was fixed
539 at 0.025 m, while the total cover depth was 0.050 m. Once again, the effects of Cl^- binding and
540 NO_3^- release were separated from that of ion-transport (i.e., diffusion) by setting the diffusion
541 coefficient of the CAC layers equivalent to that of the bulk OPC concrete. The resulting corrosion
542 delay factor is shown as a function of the surface Cl^- concentration ($C_{\text{Cl}^-}^s$); from 0.1 mol/L to 5
543 mol/L (Figure 10b). These concentrations span conditions from seawater, to exposure to deicing
544 salts, or standing seawater that is concentrated by evaporation. When surface Cl^- concentrations
545 rise beyond a limiting concentration, steel corrosion initiates very rapidly independent of the
546 cover layer composition. In the 0 mass % CN CAC mortar, the corrosion delay factor diminishes
547 to < 1 at large surface Cl^- concentrations indicating performance inferior to the OPC concrete. This
548 is due to the reduced OH^- concentration within the CAC pore solution and the high exterior Cl^-
549 concentration overwhelming the binding capacity of the system.

550
551 Similarly, CN-dosed systems demonstrate a maximum corrosion delay factor for Cl^- concentration
552 on the order of 0.5-to-1 mol/L, with a slight decrease as $C_{\text{Cl}^-}^s$ is increased. However, even at 5 mol
553 Cl^-/L , representative of exposure to concentrated seawater [89,90], the 30 % CN CAC layer delays
554 corrosion by 6.7 times relative to OPC concrete. In this case, NO_3^- release due to ACE is revealed
555 to be the critical parameter in delaying corrosion. When NO_3^- release is not considered in the 10
556 mass % CN CAC top-layer, the corrosion delay factor is halved, thus approaching that of the OPC
557 concrete at high Cl^- concentrations. **This suggests that the provision of coatings capable of ACE**
558 **is an efficient approach to – under suitable exposure conditions – more than double the service**
559 **life of concrete infrastructure.** It should be noted, however, that the conclusions of this study
560 are applicable to uncracked concrete, or concrete in which a surface penetrating crack does not
561 intersect or approach the steel reinforcement. However, due to the rapid kinetics of Cl^- uptake

562 in CAC systems [73], ACE binding is expected to exert beneficial effects even when the cover is
563 cracked. Depending on the Cl^- exposure conditions, the ACE capacity of the CAC mortar top-layers
564 is estimated to reach saturation within 10 years to 20 years. However, “mill-and-fill” operations
565 could be used to periodically replace these layers, re-enhancing the ACE capacity of such top-
566 layers. These outcomes suggest new routes to mitigate steel corrosion in concrete infrastructure.

567

568 **6. Summary and conclusions**

569 Cl^- -induced corrosion of steel embedded in reinforced concrete is a major cause of premature
570 degradation of concrete infrastructure. AFm phases present in cementitious systems are able to
571 sequester and release anions in relation to their thermodynamic preference for interlayer site
572 occupation [27,28]. This bestows AFm compounds with an ability for anion capture and exchange
573 (ACE); a novel route to mitigate Cl^- penetration and resulting corrosion. Indeed, CAC formulations
574 dosed with CN are shown to be capable of sequestering Cl^- species, while releasing corrosion
575 inhibiting NO_3^- species [19]. Precise input data of Cl^- binding and NO_3^- exchange, and ion-diffusion
576 rates are input into a multi-species Nernst-Planck model to quantitatively describe the evolutions
577 of Cl^-/OH^- and $\text{Cl}^-/\text{NO}_3^-$ ratios in the pore solution. It is noted that across all potential combinations
578 of diffusion coefficients, the effects of Cl^- binding and NO_3^- exchange are crucial in delaying the
579 onset of steel corrosion – thereby enhancing service life.

580

581 As an example, in the case of seawater exposure, the provision of CAC + CN-based top-layers is
582 estimated to increase the service life (or conversely delay the onset of steel corrosion) by a factor
583 ranging between $5 \leq d_f \leq 10$, where d_f is the delay factor (unitless). These outcomes remain
584 independent of the threshold values selected for corrosion risk indicators – i.e., commonly taken
585 as $\text{Cl}^-/\text{OH}^- \geq 0.6$ and $\text{Cl}^-/\text{NO}_3^- \leq 0.25$ – as, in general, ACE is beneficial in delaying, or preventing
586 the onset of steel reinforcement corrosion. The outcomes make a case for the use of functional
587 ACE coatings that act as more than just a physical barrier (e.g., a sealer, or a high-performance
588 concrete topping that only reduces ion-diffusion rates [91,92]) as an innovative means to mitigate
589 steel corrosion related degradation of concrete infrastructure.

590

591 **Acknowledgements**

592 The authors acknowledge financial support for this research provided by: The National Science
593 Foundation (CMMI: 1401533 and CAREER: 1235269), University of California, Los Angeles (UCLA)
594 and Yara Industrial Nitrates. The contents of this paper reflect the views/opinions of the authors,
595 who are responsible for the accuracy of datasets presented herein. This publication does not
596 construe approval or disapproval by the funding agencies and does not comprise a regulation,
597 specification, or standard. This research was carried out in the Laboratory for the Chemistry of
598 Construction Materials (LC²) and the core-Molecular Instrumentation Center at UCLA, and the
599 Engineering Laboratory at the National Institute of Standards and Technology (NIST). As such, the
600 authors acknowledge the support that has made these facilities and their operations possible.
601 The authors thank Prof. Bruce Dunn/Jonathan Lau for access to electrochemical characterization
602 tools. MB and GNS acknowledge Professor Fredrik P. Glasser (University of Aberdeen, Scotland)
603 for his insights and stimulating discussions regarding ion exchange processes.

604

605 **References**

- 606
607 [1] C.M. Hansson, The Impact of Corrosion on Society, *Metall. Mater. Trans. A.* 42 (2011) 2952–2962.
608 doi:10.1007/s11661-011-0703-2.
- 609 [2] A. Poursaeed, *Corrosion of steel in concrete structures*, 1st ed., Woodhead Publishing, 2016.
- 610 [3] U. Angst, B. Elsener, A. Jamali, B. Adey, Concrete cover cracking owing to reinforcement corrosion—
611 theoretical considerations and practical experience, *Mater. Corros.* 63 (2012) 1069–1077.
- 612 [4] S.L. Amey, D.A. Johnson, M.A. Miltenberger, H. Farzam, Predicting the service life of concrete
613 marine structures: an environmental methodology, *ACI Struct. J.* 95 (1998).
- 614 [5] G.H. Koch, M.P.H. Brongers, N.G. Thompson, Y.P. Virmani, J.H. Payer, *Corrosion cost and
615 preventative strategies in the United States*, NACE International, 2002.
- 616 [6] Federal Highway Administration, *Deficient Bridges by Highway System 2015*, (2015).
617 <http://www.fhwa.dot.gov/bridge/nbi/no10/defbr15.cfm> (accessed July 11, 2016).
- 618 [7] L. Bertolini, B. Elsener, P. Pedferri, E. Redaelli, R.B. Polder, *Corrosion of Steel in Concrete:
619 Prevention, Diagnosis, Repair*, John Wiley & Sons, 2013.
- 620 [8] Z.P. Bazant, Physical model for steel corrosion in concrete sea structures—theory, *J. Struct. Div.*
621 105 (1979) 1137–1153.
- 622 [9] J.P. Broomfield, *Corrosion of steel in concrete: understanding, investigation, and repair*, E & FN
623 Spon, London; New York, 1997.
- 624 [10] U. Angst, B. Elsener, C.K. Larsen, Ø. Vennesland, Critical chloride content in reinforced concrete —
625 A review, *Cem. Concr. Res.* 39 (2009) 1122–1138. doi:10.1016/j.cemconres.2009.08.006.
- 626 [11] D.A. Hausmann, Steel corrosion in concrete- How does it occur?, *Mater. Prot.* 6 (1967) 19–23.
- 627 [12] K.Y. Ann, N.R. Buenfeld, The effect of calcium nitrite on the chloride-induced corrosion of steel in
628 concrete, *Mag. Concr. Res.* 59 (2007) 689–697. doi:10.1680/mac.2007.59.9.689.
- 629 [13] N.S. Berke, M.C. Hicks, Predicting long-term durability of steel reinforced concrete with calcium
630 nitrite corrosion inhibitor, *Cem. Concr. Compos.* 26 (2004) 191–198. doi:10.1016/S0958-
631 9465(03)00038-6.
- 632 [14] L. Mammoliti, C.M. Hansson, B.B. Hope, Corrosion inhibitors in concrete Part II: Effect on chloride
633 threshold values for corrosion of steel in synthetic pore solutions, *Cem. Concr. Res.* 29 (1999)
634 1583–1589.
- 635 [15] M. Ormellese, M. Berra, F. Bolzoni, T. Pastore, Corrosion inhibitors for chlorides induced corrosion
636 in reinforced concrete structures, *Cem. Concr. Res.* 36 (2006) 536–547.
637 doi:10.1016/j.cemconres.2005.11.007.
- 638 [16] J.S. Reou, K.Y. Ann, The electrochemical assessment of corrosion inhibition effect of calcium nitrite
639 in blended concretes, *Mater. Chem. Phys.* 109 (2008) 526–533.
- 640 [17] A.M. Rosenberg, J.M. Gaidis, T.G. Kossivas, R.W. Previtte, A corrosion inhibitor formulated with
641 calcium nitrite for use in reinforced concrete, in: *Chloride Corros. Steel Concr.*, ASTM International,
642 1977. http://www.astm.org/DIGITAL_LIBRARY/STP/PAGES/STP27956S.htm (accessed June 5,
643 2016).
- 644 [18] J.M. Gaidis, Chemistry of corrosion inhibitors, *Cem. Concr. Compos.* 26 (2004) 181–189.
- 645 [19] M. Balonis, F.P. Glasser, Calcium nitrite corrosion inhibitor in portland cement: Influence of nitrite
646 on chloride binding and mineralogy, *J. Am. Ceram. Soc.* 94 (2011) 2230–2241. doi:10.1111/j.1551-
647 2916.2010.04362.x.
- 648 [20] M.B. Valcarce, M. Vázquez, Carbon steel passivity examined in alkaline solutions: The effect of
649 chloride and nitrite ions, *Electrochimica Acta.* 53 (2008) 5007–5015.
650 doi:10.1016/j.electacta.2008.01.091.
- 651 [21] H. Justnes, E.C. Nygaard, Calcium nitrate as a multi-functional concrete admixture, *Concrete.* 44
652 (2010) 34.

- 653 [22] V.T. Ngala, C.L. Page, M.M. Page, Corrosion inhibitor systems for remedial treatment of reinforced
654 concrete. Part 1: calcium nitrite, *Corros. Sci.* 44 (2002) 2073–2087.
- 655 [23] B. Martín-Pérez, H. Zibara, R.D. Hooton, M.D.A. Thomas, A study of the effect of chloride binding
656 on service life predictions, *Cem. Concr. Res.* 30 (2000) 1215–1223. doi:10.1016/S0008-
657 8846(00)00339-2.
- 658 [24] B.H. Oh, S.Y. Jang, Effects of material and environmental parameters on chloride penetration
659 profiles in concrete structures, *Cem. Concr. Res.* 37 (2007) 47–53.
660 doi:10.1016/j.cemconres.2006.09.005.
- 661 [25] I. Galan, F.P. Glasser, Chloride in cement, *Adv. Cem. Res.* 27 (2014) 63–97.
662 doi:10.1680/adcr.13.00067.
- 663 [26] T. Matschei, B. Lothenbach, F.P. Glasser, The AFm phase in Portland cement, *Cem. Concr. Res.* 37
664 (2007) 118–130. doi:10.1016/j.cemconres.2006.10.010.
- 665 [27] M. Balonis, The influence of inorganic chemical accelerators and corrosion inhibitors on the
666 mineralogy of hydrated portland cement systems, Ph.D. Dissertation, University of Aberdeen,
667 2010.
- 668 [28] G. Falzone, M. Balonis, G. Sant, X-AFm stabilization as a mechanism of bypassing conversion
669 phenomena in calcium aluminate cements, *Cem. Concr. Res.* 72 (2015) 54–68.
670 doi:10.1016/j.cemconres.2015.02.022.
- 671 [29] U.A. Birnin-Yauri, F.P. Glasser, Friedel's salt, $\text{Ca}_2\text{Al}(\text{OH})_6(\text{Cl},\text{OH})\cdot 2\text{H}_2\text{O}$: its solid solutions and their
672 role in chloride binding, *Cem. Concr. Res.* 28 (1998) 1713–1723. doi:10.1016/S0008-
673 8846(98)00162-8.
- 674 [30] H. Hirao, K. Yamada, H. Takahashi, H. Zibara, Chloride Binding of Cement Estimated by Binding
675 Isotherms of Hydrates, *J. Adv. Concr. Technol.* 3 (2005) 77–84. doi:10.3151/jact.3.77.
- 676 [31] R. Luo, Y. Cai, C. Wang, X. Huang, Study of chloride binding and diffusion in GGBS concrete, *Cem.*
677 *Concr. Res.* 33 (2003) 1–7. doi:10.1016/S0008-8846(02)00712-3.
- 678 [32] R.K. Dhir, M.A.K. El-Mohr, T.D. Dyer, Chloride binding in GGBS concrete, *Cem. Concr. Res.* 26
679 (1996) 1767–1773. doi:10.1016/S0008-8846(96)00180-9.
- 680 [33] T. Cheewaket, C. Jaturapitakkul, W. Chalee, Long term performance of chloride binding capacity in
681 fly ash concrete in a marine environment, *Constr. Build. Mater.* 24 (2010) 1352–1357.
682 doi:10.1016/j.conbuildmat.2009.12.039.
- 683 [34] R. Loser, B. Lothenbach, A. Leemann, M. Tuchs Schmid, Chloride resistance of concrete and its
684 binding capacity – Comparison between experimental results and thermodynamic modeling, *Cem.*
685 *Concr. Compos.* 32 (2010) 34–42. doi:10.1016/j.cemconcomp.2009.08.001.
- 686 [35] M.R. Jones, D.E. Macphee, J.A. Chudek, G. Hunter, R. Lannegrand, R. Talero, S.N. Scrimgeour,
687 Studies using ^{27}Al MAS NMR of AFm and AFt phases and the formation of Friedel's salt, *Cem.*
688 *Concr. Res.* 33 (2003) 177–182.
- 689 [36] K.O. Ampadu, K. Torii, Chloride ingress and steel corrosion in cement mortars incorporating low-
690 quality fly ashes, *Cem. Concr. Res.* 32 (2002) 893–901. doi:10.1016/S0008-8846(02)00721-4.
- 691 [37] D.P. Bentz, E.J. Garboczi, Y. Lu, N. Martys, A.R. Sakulich, W.J. Weiss, Modeling of the influence of
692 transverse cracking on chloride penetration into concrete, *Cem. Concr. Compos.* 38 (2013) 65–74.
693 doi:10.1016/j.cemconcomp.2013.03.003.
- 694 [38] D.P. Bentz, W.S. Guthrie, S.Z. Jones, N.S. Martys, Predicting Service Life of Steel-Reinforced
695 Concrete Exposed to Chlorides, *Concr. Int.* 36 (2014) 55–64.
- 696 [39] S. Jones, N. Martys, Y. Lu, D. Bentz, Simulation studies of methods to delay corrosion and increase
697 service life for cracked concrete exposed to chlorides, *Cem. Concr. Compos.* 58 (2015) 59–69.
698 doi:10.1016/j.cemconcomp.2014.12.014.

- 699 [40] M.M. Jensen, K. De Weerd, B. Johannesson, M.R. Geiker, Use of a multi-species reactive transport
700 model to simulate chloride ingress in mortar exposed to NaCl solution or sea-water, *Comput.*
701 *Mater. Sci.* 105 (2015) 75–82. doi:10.1016/j.commat.2015.04.023.
- 702 [41] E. Samson, J. Marchand, J.J. Beaudoin, Modeling the influence of chemical reactions on the
703 mechanisms of ionic transport in porous materials: An overview, *Cem. Concr. Res.* 30 (2000) 1895–
704 1902. doi:10.1016/S0008-8846(00)00458-0.
- 705 [42] O. Truc, J.-P. Ollivier, L.O. Nilsson, Numerical simulation of multi-species diffusion, *Mater. Struct.*
706 33 (2000) 566–573. doi:10.1007/BF02480537.
- 707 [43] E. Samson, J. Marchand, Modeling the transport of ions in unsaturated cement-based materials,
708 *Comput. Struct.* 85 (2007) 1740–1756. doi:10.1016/j.compstruc.2007.04.008.
- 709 [44] H. Sleiman, O. Amiri, A. Ait-Mokhtar, J.-M. Loche, Chloride transport through unsaturated
710 concrete: chloride profile simulations and experimental validation, *Mag. Concr. Res.* 64 (2012)
711 351–359. doi:10.1680/mac.9.00153.
- 712 [45] M.M. Jensen, B. Johannesson, M.R. Geiker, Framework for reactive mass transport: Phase change
713 modeling of concrete by a coupled mass transport and chemical equilibrium model, *Comput.*
714 *Mater. Sci.* 92 (2014) 213–223. doi:10.1016/j.commat.2014.05.021.
- 715 [46] T. Luping, L.-O. Nilsson, Chloride binding capacity and binding isotherms of OPC pastes and
716 mortars, *Cem. Concr. Res.* 23 (1993) 247–253.
- 717 [47] T.U. Mohammed, H. Hamada, Relationship between free chloride and total chloride contents in
718 concrete, *Cem. Concr. Res.* 33 (2003) 1487–1490. doi:10.1016/S0008-8846(03)00065-6.
- 719 [48] M. Balonis, F.P. Glasser, M. Mędała, Influence of calcium nitrate and nitrite on the constitution of
720 AFm and AFt cement hydrates, *Adv. Cem. Res.* 23 (2011) 129–143. doi:10.1680/adcr.10.00002.
- 721 [49] G. Le Saoût, V. Kocaba, K. Scrivener, Application of the Rietveld method to the analysis of
722 anhydrous cement, *Cem. Concr. Res.* 41 (2011) 133–148. doi:10.1016/j.cemconres.2010.10.003.
- 723 [50] F. Guirado, S. Galí, S. Chinchón, Quantitative Rietveld analysis of aluminous cement clinker phases,
724 *Cem. Concr. Res.* 30 (2000) 1023–1029. doi:10.1016/S0008-8846(00)00289-1.
- 725 [51] ASTM Standard C305-14. Standard Practice for Mechanical Mixing of Hydraulic Cement Pastes and
726 Mortars of Plastic Consistency, ASTM International, West Conshohocken, PA, 2014.
- 727 [52] ASTM Standard C778-13. Standard Specification for Standard Sand, ASTM International, West
728 Conshohocken, PA, 2013.
- 729 [53] K.L. Scrivener, A. Capmas, Calcium Aluminate Cements, in: P. Hewlett (Ed.), *Leas Chem. Cem.*
730 *Concr.*, 4th ed., Elsevier Science & Technology Books, 2004: pp. 713–782.
- 731 [54] M. Pérez, T. Vázquez, F. Triviño, Study of stabilized phases in high alumina cement mortars Part I
732 Hydration at elevated temperatures followed by carbonation, *Cem. Concr. Res.* 13 (1983) 759–770.
733 doi:10.1016/0008-8846(83)90077-7.
- 734 [55] PSI, GEMS Selektor, (2014). <http://gems.web.psi.ch>.
- 735 [56] D. Kulik, U. Berner, E. Curti, Modelling chemical equilibrium partitioning with the GEMS-PSI code,
736 (2004). http://www.iaea.org/inis/collection/NCLCollectionStore/_Public/36/002/36002867.pdf
737 (accessed March 1, 2015).
- 738 [57] D.A. Kulik, T. Wagner, S.V. Dmytrieva, G. Kosakowski, F.F. Hingerl, K.V. Chudnenko, U.R. Berner,
739 GEM-Selektor geochemical modeling package: revised algorithm and GEMS3K numerical kernel for
740 coupled simulation codes, *Comput. Geosci.* 17 (2012) 1–24. doi:10.1007/s10596-012-9310-6.
- 741 [58] T. Wagner, D.A. Kulik, F.F. Hingerl, S.V. Dmytrieva, GEM-Selektor geochemical modeling package:
742 TSolMod library and data interface for multicomponent phase models, *Can. Mineral.* 50 (2012)
743 1173–1195. doi:10.3749/canmin.50.5.1173.
- 744 [59] M. Balonis, F.P. Glasser, The density of cement phases, *Cem. Concr. Res.* 39 (2009) 733–739.
- 745 [60] B. Lothenbach, L. Pelletier-Chaignat, F. Winnefeld, Stability in the system CaO–Al₂O₃–H₂O, *Cem.*
746 *Concr. Res.* 42 (2012) 1621–1634. doi:10.1016/j.cemconres.2012.09.002.

- 747 [61] T.G. Jappy, F.P. Glasser, Synthesis and stability of silica-substituted hydro garnet $\text{Ca}_3\text{Al}_2\text{Si}_{3-x}\text{O}$
748 $12-4x(\text{OH})_4x$, *Adv. Cem. Res.* 4 (1991) 1–8.
- 749 [62] B.Z. Dilnesa, B. Lothenbach, G. Le Saout, G. Renaudin, A. Mesbah, Y. Filinchuk, A. Wichser, E.
750 Wieland, Iron in carbonate containing AFm phases, *Cem. Concr. Res.* 41 (2011) 311–323.
- 751 [63] B.Z. Dilnesa, B. Lothenbach, G. Renaudin, A. Wichser, E. Wieland, Stability of monosulfate in the
752 presence of iron, *J. Am. Ceram. Soc.* 95 (2012) 3305–3316.
- 753 [64] L. Filippov, F. Thomas, I. Filippova, J. Yvon, A. Morillon-Jeanmaire, Stabilization of NaCl-containing
754 cuttings wastes in cement concrete by in situ formed mineral phases, *J. Hazard. Mater.* 171 (2009)
755 731–738. doi:10.1016/j.jhazmat.2009.06.065.
- 756 [65] K.-Y. Chu, A.R. Thompson, Densities and Refractive Indices of Alcohol-Water Solutions of n-Propyl,
757 Isopropyl, and Methyl Alcohols., *J. Chem. Eng. Data.* 7 (1962) 358–360. doi:10.1021/je60014a011.
- 758 [66] C.F. Ferraris, V.A. Hackley, A.I. Avilés, Measurement of particle size distribution in portland cement
759 powder: Analysis of ASTM round robin studies, *Cem. Concr. Aggreg.* 26 (2004) 1–11.
- 760 [67] B.J. Christensen, T. Coverdale, R.A. Olson, S.J. Ford, E.J. Garboczi, H.M. Jennings, T.O. Mason,
761 Impedance Spectroscopy of Hydrating Cement-Based Materials: Measurement, Interpretation, and
762 Application, *J. Am. Ceram. Soc.* 77 (1994) 2789–2804. doi:10.1111/j.1151-2916.1994.tb04507.x.
- 763 [68] E.J. Garboczi, D.P. Bentz, Computer simulation of the diffusivity of cement-based materials, *J.*
764 *Mater. Sci.* 27 (1992) 2083–2092. doi:10.1007/BF01117921.
- 765 [69] R.S. Barneyback Jr., S. Diamond, Expression and analysis of pore fluids from hardened cement
766 pastes and mortars, *Cem. Concr. Res.* 11 (1981) 279–285. doi:10.1016/0008-8846(81)90069-7.
- 767 [70] R.L. Miller, W.L. Bradford, N.E. Peters, Specific conductance: theoretical considerations and
768 application to analytical quality control, U.S. Geological Survey, 1988.
769 <http://pubs.usgs.gov/wsp/2311/report.pdf> (accessed August 5, 2016).
- 770 [71] A.W. Adamson, A.P. Gast, Physical chemistry of surfaces, 5th ed., Wiley, 1997.
- 771 [72] G. Sergi, S.W. Yu, C.L. Page, Diffusion of chloride and hydroxyl ions in cementitious materials
772 exposed to a saline environment, *Mag. Concr. Res.* 44 (1992) 63–69.
773 doi:10.1680/macr.1992.44.158.63.
- 774 [73] G. Puerta-Falla, M. Balonis, G. Falzone, M. Bauchy, N. Neithalath, G. Sant, Monovalent ion-
775 exchange kinetics of hydrated calcium-alumino layered double hydroxides, *J. Phys. Chem. C.*
776 Submitted (2016).
- 777 [74] S. Caré, Influence of aggregates on chloride diffusion coefficient into mortar, *Cem. Concr. Res.* 33
778 (2003) 1021–1028. doi:10.1016/S0008-8846(03)00009-7.
- 779 [75] J.D. Shane, T.O. Mason, H.M. Jennings, E.J. Garboczi, D.P. Bentz, Effect of the interfacial transition
780 zone on the conductivity of portland cement mortars, *J. Am. Ceram. Soc.* 83 (2000) 1137–1144.
781 doi:10.1111/j.1151-2916.2000.tb01344.x.
- 782 [76] D.P. Bentz, O.M. Jensen, A.M. Coats, F.P. Glasser, Influence of silica fume on diffusivity in cement-
783 based materials: I. Experimental and computer modeling studies on cement pastes, *Cem. Concr.*
784 *Res.* 30 (2000) 953–962. doi:10.1016/S0008-8846(00)00264-7.
- 785 [77] N.S. Martys, Survey of concrete transport properties and their measurement, National Institute of
786 Standards and Technology, 1996. <http://fire.nist.gov/bfrlpubs/build95/PDF/b95095.pdf> (accessed
787 August 5, 2016).
- 788 [78] T.Q. Nguyen, V. Baroghel-Bouny, P. Dangla, Prediction of chloride ingress into saturated concrete
789 on the basis of a multi-species model by numerical calculations, *Comput. Concr.* 3 (2006) 401u422.
- 790 [79] E. Samson, J. Marchand, Numerical Solution of the Extended Nernst–Planck Model, *J. Colloid*
791 *Interface Sci.* 215 (1999) 1–8. doi:10.1006/jcis.1999.6145.
- 792 [80] R. Barbarulo, J. Marchand, K.A. Snyder, S. Prené, Dimensional analysis of ionic transport problems
793 in hydrated cement systems: Part 1. Theoretical considerations, *Cem. Concr. Res.* 30 (2000) 1955–
794 1960. doi:10.1016/S0008-8846(00)00383-5.

- 795 [81] H. Friedmann, O. Amiri, A. Ait-Mokhtar, Physical modeling of the electrical double layer effects on
796 multispecies ions transport in cement-based materials, *Cem. Concr. Res.* 38 (2008) 1394–1400.
797 doi:10.1016/j.cemconres.2008.06.003.
- 798 [82] A.D. MacGillivray, Nernst-Planck Equations and the Electroneutrality and Donnan Equilibrium
799 Assumptions, *J. Chem. Phys.* 48 (1968) 2903–2907. doi:10.1063/1.1669549.
- 800 [83] A.G. Dickson, C. Goyet, Handbook of methods for the analysis of the various parameters of the
801 carbon dioxide system in sea water, publisher not identified, 1994.
802 http://cdiac.esd.ornl.gov/oceans/DOE_94.pdf (accessed July 10, 2016).
- 803 [84] H.F.W. Taylor, *Cement Chemistry*, Thomas Telford, 1997.
- 804 [85] W.M. Haynes, *CRC handbook of chemistry and physics*, 96th ed., CRC Press, 2015.
- 805 [86] M. Aguayo, P. Yang, K. Vance, G. Sant, N. Neithalath, Electrically driven chloride ion transport in
806 blended binder concretes: Insights from experiments and numerical simulations, *Cem. Concr. Res.*
807 66 (2014) 1–10. doi:10.1016/j.cemconres.2014.07.022.
- 808 [87] A. Birdsall, W. Guthrie, D. Bentz, Effects of initial surface treatment timing on chloride
809 concentrations in concrete bridge decks, *Transp. Res. Rec. J. Transp. Res. Board.* 2028 (2007) 103–
810 110. doi:10.3141/2028-12.
- 811 [88] B. Lothenbach, T. Matschei, G. Möschner, F.P. Glasser, Thermodynamic modelling of the effect of
812 temperature on the hydration and porosity of Portland cement, *Cem. Concr. Res.* 38 (2008) 1–18.
813 doi:10.1016/j.cemconres.2007.08.017.
- 814 [89] N.S. Berke, M.C. Hicks, Predicting Chloride Profiles in Concrete, *Corrosion.* 50 (1994) 234–239.
815 doi:10.5006/1.3293515.
- 816 [90] M.K. Kassir, M. Ghosn, Chloride-induced corrosion of reinforced concrete bridge decks, *Cem.*
817 *Concr. Res.* 32 (2002) 139–143. doi:10.1016/S0008-8846(01)00644-5.
- 818 [91] J. Žemajtis, R. Weyers, Concrete Bridge Service Life Extension Using Sealers in Chloride-Laden
819 Environments, *Transp. Res. Rec. J. Transp. Res. Board.* 1561 (1996) 1–5. doi:10.3141/1561-01.
- 820 [92] D. Harris, J. Sarkar, T. Ahlborn, Characterization of Interface Bond of Ultra-High-Performance
821 Concrete Bridge Deck Overlays, *Transp. Res. Rec. J. Transp. Res. Board.* 2240 (2011) 40–49.
822 doi:10.3141/2240-07.
- 823